ELUCIDATION OF THE ROLE OF IKK-RELATED KINASES IN ULCERATIVE COLITIS

A THESIS SUBMITTED TO

THE GRADUATE SCHOOL OF ENGINEERING AND SCIENCE OF

BILKENT UNIVERSITY

IN PARTIAL FULFILLMENT OF THE REQUIREMENTS FOR

THE DEGREE OF

MASTER OF SCIENCE

IN

MOLECULAR BIOLOGY AND GENETICS

By

Ümran Borucu

January 2025

ELUCIDATION OF THE ROLE OF IKK-RELATED KINASES IN ULCERATIVE COLITIS

By Ümran Borucu

January 2025

We certify that we have read this thesis and that in our opinion it is fully adequate, in scope and in quality, as a thesis for the degree of Master of Science.

_____

Serkan İsmail Göktuna (Advisor)

_____

Bahar Değirmenci Uzun

_____

Aytekin Akyol

Approved for the Graduate School of Engineering and Science:

_____

Orhan Arıkan

Director of the Graduate School

ABSTRACT

ELUCIDATION OF THE ROLE OF IKK-RELATED KINASES IN ULCERATIVE COLITIS

Ümran Borucu

M.Sc. in Molecular Biology and Genetics

Advisor: Serkan İsmail Göktuna

January 2025

Ulcerative colitis is an inflammatory disease of the colon resulting from the imbalance of the inflammatory mechanisms. Its onset and development depend on multiple factors, which are not yet fully uncovered. Understanding the factors involved in the pathophysiology of ulcerative colitis is important for the management of the disease. IKK-related kinases are involved in numerous pathways in cellular signaling. They play significant roles in the modulation of the inflammatory responses. In this study, we investigated the roles played by IKK-related kinases in ulcerative colitis. We generated DSS-induced colitis mouse models in acute and chronic phases. We treated these mice with a dual IKK-related kinase inhibitor, Amlexanox, to understand the role played by these kinases on the onset and development of the condition. Moreover, we performed biochemical analyses on the samples to gain molecular insights. We observed an increased inflammatory response both phenotypically and biochemically upon inhibition of IKK-related kinases.

Keywords: Ulcerative colitis, IKK-related kinases, inflammation

ÖZET

ÜLSERATİF KOLİTTE IKK-İLİŞKİLİ KİNAZLARIN ROLÜNÜN BELİRLENMESİ

Ümran Borucu

Moleküler Biyoloji ve Genetik, Yüksek Lisans

Tez Danışmanı: Serkan İsmail Göktuna

Ocak 2025

Ülseratif kolit, kolondaki immün mekanizmaların dengesinin bozulmasından kaynaklanan iltihabi bir hastalıktır. Oluşumu ve ilerlemesi çok sayıda faktöre bağlı olup, henüz tam olarak aydınlatılamamıştır. Ülseratif kolitin patofizyolojisine katkıda bulunan faktörlerin anlaşılması hastalığın yönetimi açısından önemlidir. IKK-ilişkili kinazlar çok sayıda sinyal yolağında rol almaktadırlar. İltihabi tepkinin düzenlenmesinde önemli bir rolleri vardır. Biz bu çalışmada, IKK-ilişkili kinazların ülseratif kolitte oynadığı rolü inceledik. Çalışmamızda, DSS tarafından indüklenen akut ve kronik fazda kolit fare modelleri oluşturduk. Farelere hastalığın başlangıç ve gelişiminde IKK-ilişkili kinazların rolünü anlamak için IKK-ilişkili kinaz ikili inhibitörü olan Amlexanox uyguladık. Ayrıca, moleküler mekanizmalar hakkında daha iyi bir anlayış geliştirmek için örnekleri çeşitli biyokimyasal metotlarla analiz ettik. Hem fenotipik hem de biyokimyasal analizlerimizde IKK-ilişkili kinaz aktivitesinin susturulmasının iltihabi tepkiyi artırdığını gözlemledik.

Anahtar kelimeler: Ülseratif kolit, IKK-ilişkili kinazla, iltihap

Acknowledgment

I would like to express my profound gratitude to my supervisor, Assist. Prof. Serkan İsmail Göktuna. I would like to thank him for his guidance, support, and the opportunities he provided me in the project.

I would like to thank Dr. Tieu-Lan Chau sincerely for her valuable mentorship. I am grateful for the time and effort she spent helping me to gain valuable information and experience in my career path.

I would like to thank my committee members, Assist. Prof Bahar Değirmenci Uzun and Prof. Aytekin Akyol, deeply for their guidance in the completion of my thesis.

I would like to extend my deepest appreciation to my labmates, Eylül Kılıç and Ahmet Göktuğ Özkurt, for their support and friendship during my Master's study. Especially, I am extremely grateful to Göktuğ, my partner in this project, for his contributions to my thesis work. I would like to thank my former labmate, Servin Bagheralmoosavi, for her friendship and knowledge she was always ready to share; which helped me a lot adjusting to the lab environment during my first semester.

I would like to thank the research group of Prof. Aytekin Akyol for providing the histology results, including the Histological Activity Indexes and the H&E-stained pictures.

I would like to thank the research group of Assist. Prof. Bahar Değirmenci Uzun for their help with the qPCR experiments.

I would like to thank my friends and colleagues, Dilan Akdoğan, İlke Sarı, and Beliz Uzun, for their support and friendship.

I would like to express my greatest appreciation to my friend Cenk Günsel for being there for me and for his unconditional support every time I needed it.

Studies described in this thesis were performed with the support of TÜBİTAK ARDEB 1001 grant (221S414).

Table of Contents

List of Figures

List of Tables

Chapter 1
Introduction

1.1 Colon

The colon is a part of the digestive tract, making up one-fifth of its total length. It is positioned between the small intestine and the rectum. After up to 90% of water and the majority of the nutrients are absorbed in the small intestine, the indigestible food material reaches the colon. The colon is responsible for the absorption of remaining water, electrolytes, and vitamins, and it impels the digestive waste towards the rectum. Electrolytes are mostly absorbed actively through ion channels. An osmotic gradient is created through the absorption of the electrolytes, which aids in the absorption of water passively through osmosis. Moreover, it is responsible for not only the absorption of vitamins but also their production by the microbiota it houses. The bacteria living in the colon produce Vitamin K and B Vitamins by fermentation, which plays a crucial role in the minimization of vitamin deficiency (Azzouz & Sharma, 2023).

1.1.1 The Anatomy of the Colon

The colon is composed of four different anatomical parts: the cecum and the ascending colon, the transverse colon, the descending colon, and the sigmoid colon (Salimoglu et al., 2020) (Figure 1). The cecum constitutes the most proximal region of the colon, and it has a larger diameter than the other colonic segments. It is a blind saccular pouch, and it is connected to the ileum, creating an opening called the ileocecal valve (Wedel, 2017). The blind diverticulum, named the vermiform appendix, is located on the medial side of the cecum and is inferior to the ileocecal valve (Mahadevan, 2020). The ascending colon is located on the right side of the abdominal cavity, from the cecum to the right hepatic flexure (Salimoglu et al., 2020). The transverse colon is located between the hepatic flexure and the splenic flexure, lying intraperitoneally from right to left (Wedel, 2017). The descending colon is located on the left side of the abdomen, between the splenic flexure and the pelvic ring (Salimoglu et al., 2020). The sigmoid colon is located between the descending colon and the upper rectum,

extending through the pelvic cavity. It is S-shaped and has a high flexibility (Wedel, 2017).

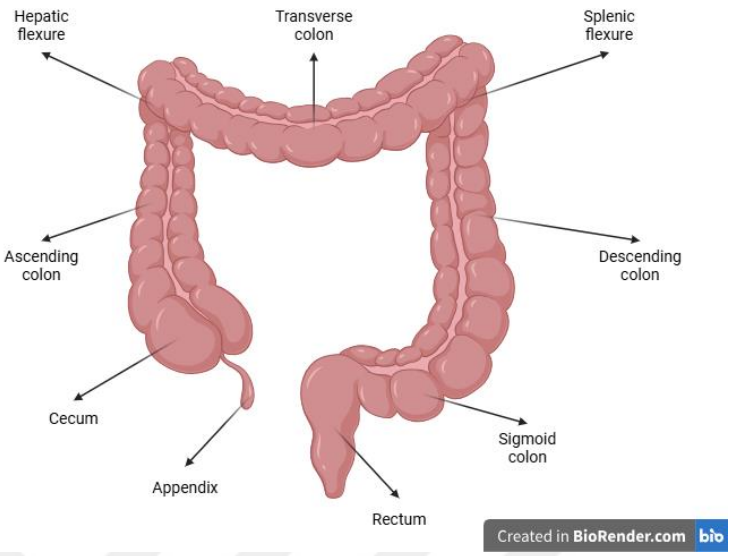

Figure 1: The general anatomy of the colon. The distinct anatomical parts of the colon, colic flexures, and rectum are depicted in the figure (Created in https://BioRender.com).

Blood supply is provided to the colon by the superior and inferior mesenteric arteries. The cecum, the ascending colon, and two-thirds of the transverse colon receive the blood supply from the superior mesenteric artery, while one-third of the transverse colon, the descending colon, and the sigmoid colon receive blood supply from the inferior mesenteric artery (Wedel, 2017).

The colonic wall comprises four distinct levels histologically: mucosa, submucosa, muscularis externa (tunisa muscularis), and serosa from the lumen outwards (Kanmaniraja et al., 2015). The mucosa contains three distinct layers: the epithelial lining, the lamina propria, and the muscularis mucosa. The epithelial lining contains single-layered epithelial cells that are responsible for absorbing water and electrolytes. This layer also houses the goblet cells, which are responsible for mucin secretion; Paneth cells, which are present only in the proximal part of the colon and produce antimicrobial peptides; and enteroendocrine cells, which are responsible for the production of hormones that regulate digestion, nutrient absorption and disposal, and appetite (Gribble & Reimann, 2019; Kanmaniraja et al., 2015; Mahon et al., 2016; Saez et al., 2023; Wedel, 2017). The lamina propria is a connective tissue layer

containing different cell types, which are fibroblasts, nerve fibers, immune cells, and capillary and lymphatic networks. Although it contains gut-associated lymphatic tissue, it lacks lymphatic vessels, which may contribute to slowing down the metastasis of some colon cancers (Kanmaniraja et al., 2015; Wedel, 2017). The muscularis mucosa is a thin muscle layer outlining the mucosa and separating it from the submucosa. It has a circular muscle layer towards the lumen side and a longitudinal muscle layer towards the outside (Salimoglu et al., 2020; Wedel, 2017). The submucosa is a loose and thick layer mostly containing connective tissue and fatty nodules. In addition to those, it contains a rich network of blood and lymph vessels, together with fibroblasts, immune cells, and nerve fiber meshes called the submucosal nerve plexus. Muscularis externa contains smooth muscle cells with two distinct layers. The inner layer, which faces the luminal side, is a circular muscle layer, while the outer layer is made up of a longitudinal muscle layer. These two layers are separated by a connective tissue space that contains the myenteric nerve plexus and a network of blood and lymph vessels. The outer longitudinal muscle layer is clustered in three major bands: the tenia omentalis, tenia libera, and tenia mesenterialis, which collectively form the teniae coli (Salimoglu et al., 2020; Wedel, 2017). The serosa is a connective tissue composed of a flattened epithelial cell layer forming a mesothelial lining. It prevents the colon from adhering to the abdominal cavity. It is absent in the cecum, the ascending colon, and the descending colon(Salimoglu et al., 2020; Wedel, 2017).

1.1.2 The Colonic Microbiota

The microorganisms living in the human body with a symbiotic relationship are named human microbiota. The colonic microbiota houses more than 70% of all the microorganisms living in the human body (Attri et al., 2022). The microbiota of the colon is vital for the formation of the colonic immune system and can play important roles in mucosal angiogenesis and the maturation of epithelial cells (Sellers & Morton, 2014). The human colonic microbiota contains more than 500 bacterial species, typically dominated by five main bacterial phyla: *Firmicutes*, *Bacteroidetes*, *Proteobacteria*, *Actinobacteria*, and *Verrucomicrobia* (Attri et al., 2022; Kelly et al., 2005). In addition to the bacteria, it also contains other microorganisms, such as

different species of archaea and fungi (Alshehri et al., 2021). The abundance and diversity of the microbial species in the colonic microbiota are crucial not only for the colonic but also for the systemic health since various metabolites produced by those microorganisms can have significant impacts on the host. The microbial composition of the colon can contribute to metabolic diseases, including insulin resistance and autoimmune diseases (Sellers & Morton, 2014). Moreover, the colonic microbiota can be vital for the prevention of the infection. Some strains living in the microbiota secrete bacteriostatic or bactericidal molecules, preventing the growth of pathogenic bacterial strains. Additionally, symbiotic microorganisms create a less favorable environment for the pathogenic microorganisms through competition for nutrients and reduction of oxygen concentration. Therefore, disturbances in the microbiota can result in the overgrowth of pathogenic bacteria such as *Clostridium difficile* (Attri et al., 2022; Sellers & Morton, 2014).

An imbalance in the colonic microbial content can result in dysbiosis, which can lead to immune-mediated diseases as it can create a pro-inflammatory environment by causing epithelial barrier dysfunction and pro-inflammatory cytokine production, such as IL-6, TNF-α, and IL1-β (Attri et al., 2022; Pop et al., 2020; Sellers & Morton, 2014). Dysbiosis and the impairment of the intestinal barrier can be associated with the development and exacerbation of inflammatory disorders such as IBD and celiac disease (Alshehri et al., 2021; L. C. H. Yu, 2018).

1.1.3 The Colonic Immunity

For colonic homeostasis, an immune balance must be maintained in the colon, preventing microbial invasion while keeping the immune response to the microbiota at a minimal level. The colonic immunity is composed of three components: the mucus barrier, the innate immunity, and the adaptive immunity. The first component of colonic immunity is the mucus layer covering the epithelial surface, termed the luminal mucus. It provides lubrication as well as a physical and chemical barrier. The mucus is mainly made up of glycoproteins termed mucins. The most prevalent mucin of the colonic mucus is MUC2, although the mucin composition and glycosylation can vary depending on the location. In addition to mucins, the luminal mucus contains anti-microbial proteins, as well as immunoglobulins. Components of the mucus, including

mucins and anti-microbial proteins, are mainly produced by Paneth cells and goblet cells, whose activity can be regulated by the microbiota. The second component is innate immunity, which can respond rapidly and non-specifically in the case of a microbial breach in the epithelium. The third one is adaptive immunity, which shows an intestine-specific acquired immune response. The immunity in the colon is mostly executed by local immune cells and works mostly independently of the systemic immune system. The immune cells working in the colon are mainly trained in a nearby location, such as the mesenteric lymph nodes or the small intestine (Saez et al., 2023; Sellers & Morton, 2014; Stefano Corazziari, 2009).

The innate immunity contains myeloid cells as well as certain non-cellular elements such as antimicrobial peptides. Its activity is not specific and is triggered by pathogen-associated molecular patterns (PAMPs) or damage-associated molecular patterns (DAMPs). These molecular patterns are recognized by pattern recognition receptors (PRRs), which are expressed by different cell types, such as intestinal epithelial cells, endothelial cells, and phagocytic cells. The response given to the activation of PRRs in the colon can change depending on the type of PRRs activated, the cell type expressing those PRRs, and the location at which they are activated. Depending on these factors, PRR activation can initiate antimicrobial peptide production, suppress inflammatory response, or drive adaptive immune response. For example, activation of PRRs on epithelial cells mostly initiates immunotolerance, while the activation on the cells of lamina propria usually drives a proinflammatory response. Innate immune cells can create host defense by producing cytokines and chemokines, initiating complement cascade, phagocytosis, and stimulating adaptive immune response through antigen presentation (Saez et al., 2023; Sellers & Morton, 2014). Notable innate immune cells that play significant roles in the innate immunity of the colon include neutrophils, macrophages, and dendritic cells. Neutrophils form the first line of defense in the case of barrier damage. They contribute to microbial elimination through phagocytosis, reactive oxygen species (ROS) generation, degranulation, and neutrophil extracellular trap (NET) formation. They undergo apoptosis or efferocytosis once their function is completed. The typical functions of macrophages are phagocytosis, cytokine production, and antigen presentation, and they can execute different functions depending on environmental factors. Macrophages can be divided into two major categories based on their function: M1 macrophages mainly contribute

to proinflammatory responses, while M2 macrophages mainly contribute to anti-inflammatory responses and tissue repair. Macrophages can be polarized into M1 or M2 phenotype depending on the environmental factor. Dendritic cells provide a crucial bridge between innate immunity and adaptive immunity due to their function as professional antigen-presenting cells (APCs). They are crucial for initiating immune response by presenting antigens to T cells and releasing various cytokines (Saez et al., 2023; Yunna et al., 2020).

The adaptive immune system involves lymphoid-originated cells that show specific and long-lasting immunity. It is composed of two components: cellular immunity and humoral immunity. Cellular immunity is mediated by T-cells, while humoral immunity is mediated by B cells (Geremia et al., 2014; Squire & Leiding, 2022). The lymphocytes located at the epithelial barrier of the intestine are named intraepithelial lymphocytes (IELs). IELs are scattered between enterocytes and hence are in immediate proximity to the antigens inside the intestinal lumen. Due to their proximity, they carry out crucial regulatory and effector functions. T-cells constitute almost the entire IEL population (Ma et al., 2019).

T-cells, the main mediators of cellular adaptive immunity, are originated from bone marrow-derived thymocyte progenitors. They develop in the thymus and become naïve T-cells, most of which further differentiate into CD4+ or CD8+ αβ effector or memory cells upon stimulation with an antigen in a secondary lymphoid organ. In addition to the αβ T-cells, a small population develops into γδ T-cells and natural killer T-cells (NKTs) (Sun et al., 2023). T-cell response originates in secondary lymphoid organs in response to innate immune system signals, which are mostly provided by the antigen-presenting cells (APCs). APCs present antigens through major histocompatibility complex (MHC), which is recognized by the T-cell receptor (TCR) of αβ T-cells. The antigen presentation to T-cells, together with the signals coming from costimulatory molecules and cytokines, results in activation, clonal expansion, and differentiation of naïve αβ T-cells into effector cells to execute their functions. A small population of T-cells turns into memory cells to provide long-term immunity. CD4+ T-cells, also termed T helper (Th) cells, play crucial roles in different aspects of immunity due to their expression of various cytokines with diverse functions. They can either initiate an inflammatory environment for protection from pathogens or tolerance for commensal microorganisms and food antigens. Th cells recognize

peptide-MHC class II complex on the surface of the APCs; and can be activated through the stimulation by peptide-MHC class II complex, costimulatory molecules, and cytokines. Upon stimulation, they can differentiate into different subsets, such as Th1, Th2, Th17, Tfh, and Treg cells. Th1 cells secrete proinflammatory cytokines and are important for protection against intracellular bacteria and viruses. Th2 cells contribute to tissue repair and protection against helminth infections. They can also play a role in chronic inflammation. Th17 cells are important for immunity against extracellular pathogens, especially in the mucosal tissue. They can also contribute to chronic inflammation and autoimmunity. Tfh cells promote B-cell proliferation and differentiation, germinal center response, and high-affinity antibody production, thus supporting humoral immunity. Tregs are crucial for the maintenance of immune tolerance and suppression of immune response. CD8+ T-cells, also termed cytotoxic T-cells (CTLs), can directly promote the death of the target cell through interaction between Fas/FasL and the secretion of cytolytic molecules perforin and granzymes, inducing apoptosis. They can also secrete pro-inflammatory cytokines such as IFN-γ and TNF-α. They are crucial for immunity against intracellular pathogens and the elimination of malignant cells. They recognize peptide-MHC class I complex (Bonilla & Oettgen, 2010; Ma et al., 2019; Sun et al., 2023).

1.2 Ulcerative Colitis

Inflammatory bowel disease (IBD) is a chronic heterogeneous group of diseases related to inflammation of the gastrointestinal tract. The etiology and pathogenesis of the disease are not fully uncovered. It can be classified into two distinct conditions based on clinical characteristics: Crohn's disease (CD) and ulcerative colitis (UC). The UC involves inflammation of the colon, which is often accompanied by ulcers. The CD can occur in any part of the gastrointestinal tract from mouth to anus, mostly involving the terminal ileum. The CD presents itself as a transmural inflammation of the entire gastrointestinal tract with a discontinuous pattern of inflammation, while the UC affects only the mucosal and submucosal layer of the colon with a continuous pattern of inflammation (Ho et al., 2020; Saez et al., 2023).

The UC has a high prevalence in high-income countries with a stable or decreasing incidence rate in recent years, and its incidence rate is increasing in middle-income

and low-income countries. It does not show a sex predominance. Although it can occur at any age, its onset is most commonly seen between ages 30 and 40 (Kobayashi et al., 2020; Le Berre et al., 2023).

The symptoms of UC involve bloody diarrhea, abdominal pain, urgency, tenesmus, and hematochezia. It can cause the distortion of the crypt architecture, depletion of goblet cells, mucosal atrophy, and submucosal fibrosis. It increases the likelihood of colorectal cancer development later in life. It is a lifelong disease showing periods of relapse and remission (Ho et al., 2020; Le Berre et al., 2023). The risk factors for developing UC involve genetics, diet, and gut microbiota. 8-14% of UC patients have a family history of IBD, and first-degree relatives of UC patients have a four times higher risk of developing the disease. Based on genome-wide association studies, certain loci have been identified to be related to IBD. These IBD-associated loci contain genes with various functions, such as innate and adaptive immunity, cytokine signaling, epithelial barrier function, and response to microbial molecules. Smoking is known to have a protective effect against UC, with active smokers having a lower risk of developing UC compared to former and non-smokers, although the mechanism behind this phenomenon is not known (Kobayashi et al., 2020; Ungaro et al., 2017).

1.2.1 The Pathogenesis of Ulcerative Colitis

The exact etiology of UC remains unknown. However, it is sustained in genetically susceptible individuals due to an impaired immune response to gut microbiota. It is linked to a breach of the epithelial barrier, and the deficiency of inflammatory response resolution, together with a disruption of the tolerance for the microbiota, leading to the persistence of the disease (Saez et al., 2023).

1.2.1.1 Dysbiosis

The composition of the human gut microbiota highly influences the onset of diseases and human health. The balance of the microbial composition is crucial for a healthy gastrointestinal tract (Alshehri et al., 2021). Dysbiosis can be defined as the alterations in the microbiota, disrupting the balance and causing abnormal host response (Singh et al., 2016). Dysbiosis of the colon has been shown to be linked to UC, although it is

not known if the dysbiosis is a cause or a result of inflammation related to UC. A decline in the biodiversity of the colonic microbiota has been observed in patients with UC. The abundance of some bacteria, such as *Roseburia hominis* and the members of Firmicutes, was reported to decrease in UC patients, while the abundance of some other species, such as Gammaproteobacteria and Enterobacteriaceae, was reported to increase. However, the effect of the change in the abundance of individual bacterial species is not well understood. Although single fecal transplantation to UC patients does not promote recovery, repeated fecal transplantation and even treatment with bacterial metabolites, such as short-chain fatty acids (SCFAs), have been shown to improve the condition in experimental setups (Kobayashi et al., 2020; Ungaro et al., 2017).

1.2.1.2 The Immune System Dysfunction

Abnormal response of innate and adaptive immunity plays a crucial role in UC pathogenesis. The disease onset is thought to be related to damage to the epithelial barrier, causing the release of DAMPs and PAMPs, which trigger an innate immune response. This damage can be caused by an infection, a chemical compound, or a metabolic alteration due to different reasons, such as changes in the diet. Following the initial damage, deficiency in the resolution of the immune response is suggested to be the main factor perpetuating the condition (Saez et al., 2023; Ungaro et al., 2017).

Neutrophils are the first cells that respond to the signals resulting from the initial damage. Their inflammatory action can not only amplify the inflammatory response but also cause tissue damage due to the production of matrix metalloproteases, NETs, reactive oxygen species, and proinflammatory cytokines, such as IL-8 and TNF-α. Proinflammatory monocytes and macrophages are also recruited to the colon due to the damage-related signals and proinflammatory cytokines produced by neutrophils. These macrophages have an elevated expression of proinflammatory cytokines, such as TNF-α, IL-1β, and IL-6. The recruited monocytes also differentiate into proinflammatory effector cells, contributing to the immune response. In addition to proinflammatory macrophages, M2-like macrophage polarization promotes tissue repair, contributing to the remission periods of UC (Qu et al., 2025; Saez et al., 2023). Dendritic cells are antigen-presenting cells that bridge innate and adaptive immunity.

In the healthy state of the colon, they primarily collect food antigens and promote a tolerogenic environment upon recognition of the commensal microorganisms. During UC, dendritic cells can show an abnormal phenotype, contributing to the inflammatory response by releasing proinflammatory cytokines, such as IL-6, IL-12, and IL-18 (Saez et al., 2023).

The aberrant function of the innate immune cells, especially APCs, in UC drives the abnormal activity of T-cells, perpetuating the inflammatory response due to the increased cytokine and chemokine release. Although the activity of CD8+ T-cells can affect the course of the disease, the activity of CD4+ T-cells is more important for UC pathogenesis. Traditionally, UC is considered a Th2-mediated disease with an elevated level of IL-4, IL-5, and IL-13. Additionally, elevated expression of many key cytokines, such as TNF-α, IL-17, IL-23, and IL-9, can be observed in UC. The elevated level of IL-17 in UC indicates the involvement of Th17 cells in addition to the traditionally accepted Th2-mediated immunity. Additionally, the intestinal mucosa of UC patients shows an elevated level of Treg cells, which suppress excessive immune response through the production of anti-inflammatory cytokines IL-10 and TGF-β. However, the effector T-cells in the lamina propria of the UC patients were observed to have a decreased responsiveness to Treg cell activity (Alshehri et al., 2021; Geremia et al., 2014; Ho et al., 2020; Yue et al., 2024). Although T-cell activity plays a superior role in terms of aberrant adaptive immunity in UC, perturbations in humoral immunity also have a role. UC patients show an elevated concentration of IgM, IgA, and IgG; especially, the IgG1 antibody level was observed to be disproportionately elevated in UC patients (Ungaro et al., 2017; Yue et al., 2024).

1.2.1.3 Oxidative Stress

The oxygen-containing compounds that have a higher reactivity than oxygen itself and can cause oxidative damage to various biomolecules, such as proteins, lipids, and nucleic acids, are termed reactive oxygen species (ROS). Some compounds that can be defined as ROS include superoxide, hydrogen peroxide, hydroxyl radical, hypochlorous acid, ozone, and singlet oxygen. In the gastrointestinal tract, sources of ROS include microbiota, byproducts of aerobic metabolism in mitochondria, and immune cells during inflammation. During inflammation, a substantial amount of ROS

is produced by activated neutrophils and macrophages since ROS can contribute to defensive function due to their bactericidal effect. Cells have antioxidant systems that can scavenge and neutralize ROS to counteract the harmful impacts. Oxidative stress occurs when there is an imbalance between ROS production and the antioxidant system. It is closely linked to inflammation, and known to be involved in the development and exacerbation of UC. The abundance of immune cell infiltration to the colon during UC causes oxidative stress, which damages important macromolecules, contributing to cell injury and mucosal barrier damage (Krzystek-Korpacka et al., 2020; Li et al., 2016; Wang et al., 2016; Y. Yu et al., 2024).

The antioxidant enzymes that act as the first line of defense against ROS include but are not limited to superoxide dismutase (SOD), catalase (CAT), and glutathione peroxidase (GPx). These enzymes neutralize the ROS and prevent the formation of new ones (Krzystek-Korpacka et al., 2020). SOD catalyzes the conversion of superoxide radicals into molecular oxygen and hydrogen peroxide (Younus, 2018). Although less reactive than superoxide radicals, the resulting hydrogen peroxide contributes to oxidative stress, and different enzymes, such as CAT and GPx, can neutralize it. CAT can convert hydrogen peroxide into water and oxygen in a two-step reaction (Nandi et al., 2019). GPx uses glutathione as a hydrogen donor and reduces hydrogen peroxide and organic hydroperoxides (Blanco & Blanco, 2022). In addition to the antioxidant enzymes, the antioxidant defense system contains free radical scavenger molecules, such as glutathione (GSH), bilirubin, vitamins A, E, C, and carotenoids. These molecules donate electrons to ROS to neutralize them (Krzystek-Korpacka et al., 2020).

The NRF2 gene is crucial for antioxidant response. In fact, it is referred to be the "master regulator" of the antioxidant response due to its modulatory effect on the expression of various genes that are crucial for the antioxidant response. In addition to the members of the antioxidant system, it modulates the expression of various other genes involved in important functions, such as inflammatory responses, tissue remodeling, carcinogenesis, and metastasis. It regulates the human Antioxidant Response Element (ARE) positively, which promotes the expression of numerous antioxidant genes (Bellezza et al., 2018).

Oxidative stress can be measured using various biomarkers. The molecules that can be used as oxidative stress biomarkers include ROS themselves, molecules that are created as oxidation products due to the interaction with ROS in the microenvironment, ROS-generating enzymes, and elements of the antioxidant defense system. The direct measurement of ROS in the microenvironment is a valuable tool, although it is a complex task due to the short half-life of those compounds. Examples of these biomolecules include hydrogen peroxide, hypochlorous acid, and superoxide radicals. Lipid oxidation products, such as HNE and MDA, DNA oxidation products, such as 8oxodG and 5-chlorocytosine, and protein oxidation products, such as carbonyls and 3-chloro-tyrosine, can be utilized to assess the number of molecules that are created due to ROS. ROS-generating enzymes that can be used to measure oxidative stress involve MPO, NOS, and NOX. Finally, the elements of the antioxidant system that can be used as an oxidative stress marker involve SOD, CAT, GPx, and glutathione (Marrocco et al., 2017).

1.2.1.4 The Barrier Dysfunction

The mucus layer and the epithelial lining beneath it maintain the barrier function on the colon, preventing the microorganisms on the lumen from a possible invasion. The integrity of the epithelial barrier is preserved by the apical junction complex, which contains tight junctions, adherens junctions, and desmosomes. In addition to being a physical barrier preventing microbial invasion, it also exerts a chemical barrier function due to the bactericidal compounds secreted by epithelial cells, such as defensins. In a healthy state, only a few luminal antigens are capable of passing to lamina propria due to the functional intestinal barrier. The existing immune tolerance mechanisms are able to tolerate these few antigens within the lamina propria (Geremia et al., 2014; Kobayashi et al., 2020). Defects in the mucus barrier and the epithelial barrier are known to be strongly connected to UC. Alterations in the expression of tight junction proteins contribute to impaired barrier function in UC. Alteration of the goblet cell function, leading to a reduction in the thickness of the mucus layer, is also known to be involved in UC pathogenesis. Defects in the intestinal barrier lead to an increase in the amount of luminal antigens that can breach the barrier, causing the fail of the tolerance mechanisms within the lamina propria. This results in the stimulation of the

local immune cells and infiltration of further immune cells due to the cytokines and chemokines produced. Subsequently, it causes the development and exacerbation of the immune response (Kobayashi et al., 2020; Ungaro et al., 2017).

1.2.2 Mouse Models of Ulcerative Colitis

Murine models have been essential to studying IBD pathogenesis and potential therapeutic options for it. Many different models were developed for IBD research, including transgenic and gene-targeted strains, adoptive T-cell transfer, spontaneous models, and chemically induced models. Among these, chemically induced models are the most commonly used due to the uncomplicated protocols resulting in a rapid inflammation onset. When chosen suitably, chemically induced animal models can be valuable tools since they replicate some major immunological and histopathological aspects of IBD in humans, although none of these models represent all aspects of human IBD. The most widely used chemicals to induce IBD are trinitrobenzene sulfonic acid (TNBS) and dextran sodium sulfate (DSS). In murine models, the inflammation induced by DSS mirrors human UC better, while the inflammation induced by TNBS mirrors human CD better. Moreover, the UC model created with DSS is more flexible than the other chemically induced models. By changing the concentration and treatment frequency of DSS, acute, chronic, and relapsing models can be obtained. Moreover, it can be combined with other chemicals to create different models. For example, a colitis-associated colorectal cancer model can be obtained by coupling DSS treatment with Azoxymethane (AOM) injection (Wen et al., 2023; Wirtz et al., 2017; Yang & Merlin, 2024).

DSS is a negatively charged polysaccharide. Its molecular weight can vary between 5 kDa to 1400 kDa. The molecular weight of DSS determines its ability to penetrate through the intestinal mucus layer. The lower the molecular weight, the easier it is to penetrate through the mucosal layer. Furthermore, DSS creates nanovesicles in the colonic lumen by forming complexes with medium-chain-length fatty acids (MCFAs). These nanovesicles lead to damage to the distal colon by fusing with the colonocyte membranes. DSS with higher molecular weight is more prone to form complexes with MCFAs. Although the DSS-MCFA nanovesicles damage epithelial cells, the increased size decreases their permeability. Considering these factors, medium-sized DSS with

a molecular weight of 40 kDa has been observed to have the highest capacity to promote colitis. Moreover, the intense microbial population of the colon makes it rich in microbial-derived MCFAs, which can form complexes with DSS, damaging the epithelial lining. Therefore, the inflammation triggered by DSS is localized more in the colon rather than the small intestine (Yang & Merlin, 2024).

The exact mechanism behind the induction of colitis through DSS treatment is not fully uncovered. However, it is known that sulfate groups of DSS can damage the mucus layer, making it more permeable to luminal antigens, including pathogenic microorganisms. Moreover, it is known to damage epithelial cells, disturbing the epithelial lining. Therefore, it is known to impair the intestinal barrier, causing the luminal antigens to cross to the underlying tissue layers, stimulating a proinflammatory response. This response is associated with various inflammatory mediators, such as cytokines, chemokines, ROS, nitric oxide (NO), and components activating the complement system. At the acute stage of DSS-induced colitis, the inflammation is mainly caused by disruption of the epithelial barrier and innate immune responses. At this stage, T-cell-mediated adaptive immunity is not required for the development of inflammation, as evidenced by the experiments with immunodeficient mice. However, the studies done with wild-type mice show that the presence of T-cell response exacerbates the inflammation. Moreover, DSS models with wild-type mice show a Th1-polarized response during the acute phase, while the response becomes Th1/Th2 mixed during the chronic phase (Yang & Merlin, 2024).

1.3 IKK-Related Kinases

The members of IKK-related kinases are IKKε (also called IKBKE) and TBK1 (also called NAK), which show 64% homology with each other and 27% homology with the classical IKKs (IKKα and IKKβ). Even though they show structural homology with classical IKKs, they are not part of the classical IKK complex, which activates NF-κB signaling. Although they were shown to be able to activate NF-κB when overexpressed in an *in vitro* setting, they are not essential for NF-κB signaling. In contrast to classical IKKs, they can phosphorylate only one phosphoacceptor site of IκB instead of two, thus failing to start the signaling cascade (Häcker & Karin, 2006; Llona-Minguez et al., 2013). However, they can play an important role in the induction

of NF-κB-mediated response. Phosphorylation of NF-κB subunit p65/RelA S536 is essential for the second phase of NF-κB activation, determining the strength and duration of the signaling response. This phosphorylation can be done not only by classical IKKs but also by IKK-related kinases. Moreover, IKKε can phosphorylate p65 at S468, enhancing its activity. In conclusion, although IKK-related kinases are not a part of the classical IKK complex that can directly activate NF-κB signaling, they still play important roles in the regulation of NF-κB signaling cascade (Clément et al., 2008).

1.3.1 IKK-Related Kinases in Antiviral Response

Viral infection or activation of certain Toll-like receptors (TLRs) causes the activation of IKKε and TBK1. When activated, IKKε and TBK1 form complexes with a scaffold protein, such as TRAF3, TANK, and NAP1, and phosphorylate the interferon (IFN) regulatory factors IRF3 and IRF7 at their key C-terminal amino acids. In response to this phosphorylation, IRF3 and IRF7 form homo- or heterodimers, which can localize to the nucleus and induce transcription of type I IFN (IFN-I) genes, such as IFN-α and IFN-β. Thus, IKK-related kinases are crucial for antiviral response. Initial activation of IFN-I genes enhances the expression of secondary IFN-I and IFN-I-responsive genes, resulting in a significant IFN-I response. The level of IRF-7 is controlled at the transcriptional level, while IRF3 is dormant in the cytosol. Notably, IRF7 is one of the IFN-I-responsive genes, creating a positive feedback loop (Häcker & Karin, 2006).

Various scaffolding effectors, such as SINTBAD, HSP90, NAP1, TANK, TRAF3, TRADD, and FADD can regulate the kinase activity of IKK-related kinases. Moreover, in response to infection by RNA viruses, IKK-related kinases can be activated by intracellular RNA receptors, including RIG-I and MDA-5. Cytosolic DNA receptors, such as DAI, can also activate signaling through IKK-related kinases (Clément et al., 2008).

1.3.2 IKK-Related Kinases in Oncogenesis

In addition to their roles in inflammatory responses, IKKε and TBK1 are also known to be involved in the development and progression of cancer. They can play a role in

Ras-induced oncogenesis. TBK1 is involved in the Ras-like-guanine nucleotide exchange factor pathway, which is necessary for Ras-induced transformation (Clément et al., 2008).

IKKε is involved in many different signaling pathways that play role in tumorigenesis. It can activate AKT by directly phosphorylating it at S473 and T308. AKT activation by IKKε can happen both in PI3K-dependent and independent fashion. It can elevate c-Myc activity by enhancing the signaling through the AKT/GSK3β/c-Myc cascade. Moreover, IKKε also functions downstream of AKT, and activation of AKT can promote IKKε expression. In addition to its role in AKT signaling, IKKε is also shown to be capable of promoting the expression of YAP1 and TEAD2, hence enhancing the activity of the Hippo pathway, which has regulatory roles on cell proliferation, apoptosis, and cell differentiation. Furthermore, it can regulate β-Catenin activity, contributing to Wnt signaling (Yin et al., 2020).

On the other hand, IRF-3 has tumor suppressor properties due to its function in apoptosis. It can contribute to apoptosis in a p53-independent manner by activating genes, such as NOXA, TRAIL, and ISG56, which causes protein synthesis abrogation and apoptosis. IRF-3 can also inhibit cancer cell growth by activating p53 indirectly through the promotion of the PML gene transcription. IRF-7 has been shown to have both oncogenic and tumor suppressor potential. It was shown to promote tumor formation in nude mice, suggesting an oncogenic role. It was also observed to be associated with the downregulation of proangiogenic/metastatic genes, including VEGF and MMP2. Additionally, it increases the antitumor function of macrophages by upregulating genes such as CD80, ISG56, IL12p35, IL15, and TRAIL (Clément et al., 2008).

1.4 Aim of the Study

IKK-related kinases are known to be involved in numerous pathways with different functions, including inflammatory response. They are key regulators in Type I IFN response and are involved in the regulation of NF-κB signaling, another crucial pathway in inflammatory response. However, the role they play in cellular signaling is not limited to these pathways. UC is an inflammatory condition that involves various cell populations and dysregulation of numerous pathways. Considering the key roles

they play in various pathways, IKK-related kinases might be involved in the onset and development of UC in different ways. In this study, we aim to understand the role played by IKK-related kinases in UC onset and development. For this purpose, we employed DSS-incuded colitis mouse model, in which we pharmacologically silence the activity of IKK-related kinases. To evaluate the role of IKK-related kinases in different stages of the disease, we generated both acute and chronic phase colitis models. Furthermore, we employed various biochemical analyses, aiming to understand their role at the molecular level.

Chapter 2

Materials and Methods

2.1 Materials

The materials used in this study are described below.

2.1.1 Chemicals and Reagents

A list of chemicals and reagents used in this study can be seen in Table 1.

Table 1: Chemicals and reagents used in this study

Product Name	Catalog Number	Company
30% Acrylamide/Bis Solution 29:1	1610156	Bio-Rad
Glycerol 85%	927.023.1000-1L	IsoLab
Trizma base	T1503-1KG	Sigma-Aldrich
Ethylenedinitrilotetraacetic acid disodium salt dihydrate (EDTA)	1.08421.1000	Merck
Dodecyl sulfate sodium salt	8.22050.1000	Merck
Ammonium persulfate (APS)	A2941,0500	AppliChem
TEMED	A1148,0100	AppliChem
Glycine	927-032-1000-1KG	IsoLab
Sodium Chloride	969.033.1000-1KG	IsoLab
Methanol	947.046.2500-2.5L	IsoLab
Ethanol Absolute	920.026.2500-2.5L	IsoLab
2-Propanol	961.023.2500-2.5L	IsoLab
Tween 20	39796.51	Serva
Bovine Serum Albumin (BSA)	Sc-2323	ChemCruz
Hydrochloric acid	30721-2.5L	Sigma-Aldrich
Sodium hydroxide pellet	06203	Sigma-Aldrich
Acetic Acid (Glacial) 100 % Anhydrous	901.013.2500-2.5L	IsoLab
β-Mercaptoethanol	A1108,0250	AppliChem

Bromophenol Blue	0449-100G	Amresco
Sodium Azide	S2002-5G	Sigma-Aldrich
Clarity Western ECL Substrate	1705060	Bio-Rad
SuperSignal West Femto Maximum Sensitivity Substrate	34095	Thermo Scientific
TRIpure Total RNA Extraction Reagent	EP013	ELK Biotechnology
Hank's Balanced Salt Solution (HBSS)	BE10-547F	Lonza
cOmplete Protease inhibitor cocktail tablets	11697498001	Roche
UltraPure 0.5M EDTA, pH 8.0	15575-038	Invitrogen
Dextran sulfate sodium (DSS)	DB001	TdB Labs
Ponceau S	A1405,0025	AppliChem
Formaldehyde Solution About 37% for analysis	923.015.2500-2.5L	IsoLab
Paraformaldehyde	1.04005.1000	Merck
PageRuler Prestained Protein Ladder	26616	Thermo Scientific
Süt Tozu (Milk powder)	-	Pınar
PMSF	A0999,0025	AppliChem
EGTA	11290.01	Serva
Trizma Hydrochloride	T-3253	Sigma-Aldrich
Triton X-100	A1388,0500	AppliChem
Sodium orthovanadate	S6508-50G	Sigma-Aldrich
Sodium Fluoride	1.06449.0250	Merck
Tetrasodium pyrophosphate	P-8010	Sigma-Aldrich
Dimethylsulfoxide (DMSO)	M.6323.0100	Genaxxon Bioscience
Amlexanox	A2401	Tokyo Chemical Industry
LightCycler 480 SYBR Green I Master	04887352001	Roche

2.1.2 Kits

A list of the kits used can be seen in Table 2.

Table 2: Kits used in this study

Product Name	Catalog Number	Company
C-Series Mouse Inflammation Antibody Array C1	AAM-INF-1-8	RayBiotech
Hydrogen Peroxide (H2O2) Colorimetric Assay Kit	E-BC-K102-S	Elabscience
Nitric Oxide (NO) Colorimetric Assay Kit	E-BC-K035-S	Elabscience
Malondialdehyde (MDA) Colorimetric Assay Kit (TBA Method)	E-BC-K025-S	Elabscience
Glutathione Peroxidase (GSH-Px) Activity Assay Kit	E-BC-K096-S	Elabscience
Catalase (CAT) Activity Assay Kit	E-BC-K031-S	Elabscience
Total Superoxide Dismutase (T-SOD) Activity Assay Kit (WST-1 Method)	E-BC-K020-M	Elabscience
PrimeScript RT Master Mix (Perfect Real Time)	RR036A	Takara
Pierce BCA Protein Assay Kit	23227	Thermo Scientific

2.1.4 Buffers

A list of buffers used in this study and their formulations are listed in Table 3.

Table 3: Buffers used in this study and their formulations

Buffer Name	*Formulation*
Tissue lysis buffer 2x	100 mM Tris-HCl, 500 mM NaCl, 0.2 mM EGTA, 2% Triton-X, 1% NP40, 20% Glycerol, 0.5 mM Tetrasodium Pyrophosphate
Tissue lysis buffer 1x	5 mL Tissue lysis buffer 2x, 500 µL NaF, 500 µL Sodium orthovanadate, 100 µL β-

	glycerophosphate, 10 µL DTT 1M, 200 µL PMSF 0.1M, cOmplete protease inhibitor tablet, ddH2O to complete 10 mL
Phosphate Buffer Saline (PBS) 10x	17.02 g Na2HPO4, 80 g NaCl, 2 g KCl, 2 g KH2PO4, ddH2O up to 1 L, pH= 6.87
4% PFA	40 g PFA, 1x PBS up to 1L, pH=7.00

2.1.5 qPCR Primers

A list of qPCR primers used in this study is listed in Table 4.

Table 4: qPCR primers with sequences used in this study

Gene name	Sequence
mFizz-1 (Retnla) - F	CTCCACTGTAACGAAGACTC
mFizz-1 (Retnla) - R	GCAGTGGTCCAGTCAACGA
mCcl22-F	AGGTCCCTATGGTGCCAATGT
mCcl22-R	CGGCAGGATTTTGAGGTCCA
mArg1-F	CTCCAAGCCAAAGTCCTTAGAG
mArg1-R	AGGAGCTGTCATTAGGGACATC
mCcl5-F	GCTGCTTTGCCTACCTCTCC
mCcl5-R	TCGAGTGACAAACACGACTGC
mCd86 - F	CATGGGCTTGGCAATCCTTA
mCd86 - R	AAATGGGCACGGCAGATATG
mCd80 - F	GCAGGATACACCACTCCTCAA
mCd80 - R	AAAGACGAATCAGCAGCACAA
mGclc-F	GGGGTGACGAGGTGGAGTA
mGclc-R	GTTGGGGTTTGTCCTCTCCC
mGpx1-F	AGTCCACCGTGTATGCCTTCT
mGpx1-R	GAGACGCGACATTCTCAATGA
mGsr-F	GGGTGGCACTTGCGTGAATG
mGsr-R	GGCGGCTCACATAGGCATCCC
mHmox1-F	AAGCCGAGAATGCTGAGTTCA

mHmox1-R	GCCGTGTAGATATGGTACAAGGA
mPtgs2-F	TGAGCAACTATTCCAAACCAGC
mPtgs2-R	GCACGTAGTCTTCGATCACTATC
mIfn-B-F	AGCTCCAAGAAAGGACGAACAT
mIfn-B-R	GCCCTGTAGGTGAGGTTGATCT
mCd163-F	GGTGGACACAGAATGGTTCTTC
mCd163-R	CCAGGAGCGTTAGTGACAGC
mCd4-F	AGGTGATGGGACCTACCTCTC
mCd4-R	GGGGCCACCACTTGAACTAC
mCd8a-F	AAGAAAATGGACGCCGAACTT
mCd8a-R	AAGCCATATAGACAACGAAGGTG
mCd68-F	TGTCTGATCTTGCTAGGACCG
mCd68-R	GAGAGTAACGGCCTTTTTGTGA
mF4/80-F	CTTTGGCTATGGGCTTCCAGTC
mF4/80-R	GCAAGGAGGACAGAGTTTATCGTG
mFoxp3-F	CCCATCCCCAGGAGTCTTG
mFoxp3-R	ACCATGACTAGGGGCACTGTA
mGr1-F	GCAATGCAGCAGTTCCCACT
mGr1-R	ATTGAATGGATCATCAGAGAAAGGTC
mPtprc(B220)-F	ATGGTCCTCTGAATAAAGCCCA
mPtprc(B220)-R	TCAGCACTATTGGTAGGCTCC
mCd11c-F	CTGGATAGCCTTTCTTCTGCTG
mCd11c-R	GCACACTGTGTCCGAACTCA
mCxcl1-F	TATCGCCAATGAGCTGCG
mCxcl1-R	GGATGTTCTTGAGGTGAATCCC
mCxcl11/I-TAC-F	GCTCAAGGCTTCCTTATGTTCAAAC
mCxcl11/I-TAC-R	CTTTGTCGCAGCCGTTACTCG
mG-CSF-F:	TTGGCAACATCCAGCTGAAG
mG-CSF-R:	GCAGGCTCTATCGGGTATTTC
mIfn-G-F	TTACTGCCACGGCACAGTCA
mIfn-G-R	AGTTCCTCCAGATATCCAAGAAGAGA
mIl-1b-F	GTGGCTGTGGAGAAGCTGTG
mIl-1b-R	GAAGGTCCACGGGAAAGACAC

mIl-2-F:	GATGAACTTGGACCTCTGCG
mIl-2-R:	CATCATCGAATTGGCACTCA
mIl-4-F	ACAGGAGAAGGGACGCCAT
mIl-4-R	GAAGCCCTACAGACGAGCT
mIl-6-F	GTATGAACAACGATGATGCACTTG
mIl-6-R	ATGGTACTCCAGAAGACCAGAGGA
mIl-10-F	GGTTGCCAAGCCTTATCGGA
mIl-10-R	ACCTGCTCCACTGCCTTGCT
mIl-12p35-F	CACGCTACCTCCTCTTTTTG
mIl-12p35-R	CAGCAGTGCAGGAATAATGTT
mIl-17-F	TTTAACTCCCTTGGCGCAAAA
mIl-17-R	CTTTCCCTCCGCATTGACAC
mNos2-F	CCCTCCTGATCTTGTGTTGGA
mNos2-R	CAACCCGAGCTCCTGGAAC
mTnfrsf1b-F	GTCTGGAACCAGTTTCGTACAT
mTnfrsf1b-R	ACACTCGGTTCTGCTGTTTAG
mCcl24-F:	ATTCTGTGACCATCCCCTCAT
mCcl24-R:	TGTATGTGCCTCTGAACCCAC

2.2 Methods

2.2.1 Ulcerative Colitis Animal Models

All the protocols related to animal experimentation used in this study are reviewed and approved by the Bilkent University Animal Ethics Committee, and the animals used in this study were maintained at the Bilkent University Animal Facility.

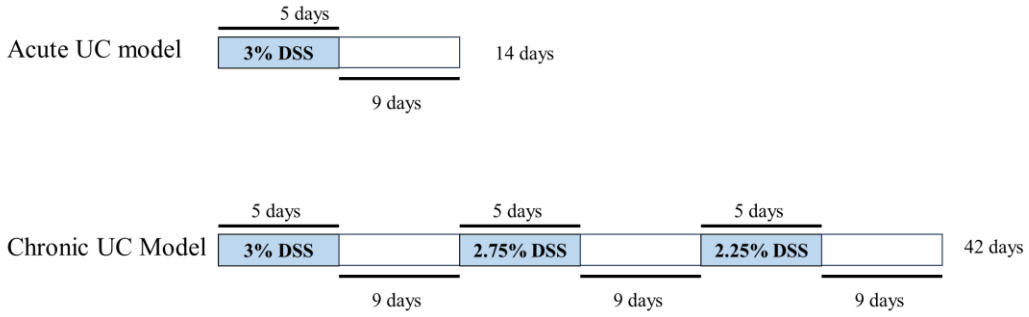

Figure 2: Experimental design scheme for the DSS treatment of the UC models.

For this study, 8-12 weeks old male FVB/N mice were used. To induce ulcerative colitis, mice were supplied with drinking water containing Dextran sulfate sodium (DSS) *ad libitum*. For the acute ulcerative colitis model, mice were given drinking water containing 3% DSS for 5 days. At the end of the fifth day, it was replaced with regular drinking water for 9 days for the recovery process. The mice were sacrificed after their recovery was completed. For the chronic ulcerative colitis model, 3 DSS-recovery cycles were employed. All of these cycles comprised 5 days of DSS treatment through drinking water, followed by 9 days of the recovery process with regular drinking water. For the first cycle, 3.00% DSS; for the second cycle, 2.75% DSS; and for the third cycle, 2.25% DSS was used. The mice were sacrificed after the last recovery was completed. A schematic representation of the DSS treatment can be seen in Figure 2.

2.2.2 Pharmacological Inhibition of IKK-related Kinases

To inhibit IKK-related kinases pharmacologically in mice, TBK1/IKBKE dual inhibitor Amlexanox was used. 500 mM Amlexanox stock solution was prepared by dissolving Amlexanox powder in DMSO, which was later diluted with vehicle Solution (250 M Tris-HCl, pH: 7.4) to 25 mM freshly before use. For the experiment group, 50 mg/kg Amlexanox was given to mice daily through gavaging starting from day zero to the end of the experiment. For the control group, the Vehicle solution containing the same amount of DMSO as the experiment group was given to mice daily through gavaging starting from day zero to the end of the experiment. Each group contains 6 mice that have undergone the same DSS treatment in both experiments.

2.2.3 Clinical Scoring of the Animals

To follow the health status of the animals, a clinical score was assigned to each mouse daily. A modified version of the Disease Activity Index (Azuma et al., 2008), described in the literature, was used to assign and calculate the clinical scores. In this modified version, the clinical scores were calculated using the weight loss percentage, fecal consistency, and observable fecal blood content. The scoring system explained in Table 5 was used for scoring, and the average of these three criteria was calculated to obtain the final clinical score.

Table 5: Clinical Scoring System to Evaluate the Severity of Colitis in Mice

Score	Weight loss (%)	Fecal consistency	Rectal bleeding/ Fecal occult blood
0	0	Normal	No blood
1	1-5	Slightly soft	Observable blood in the feces (+)
2	5-10	Soft	Observable blood in the feces (++)
3	10-15	Very soft	Observable blood in the feces (+++)
4	>15	Diarrhea	Gross rectal bleeding

2.2.4 Dissection& Tissue Collection

The mice were put under anesthesia with isoflurane and euthanized by terminal blood collection.

The colon was extracted, and its size was measured using a caliper. The fecal matter was removed by flushing the colon with cold 1x PBS. The cleaned colon was divided lengthwise into two pieces, one of which was Swiss-rolled for the histopathological analysis, and the other one was minced for whole mucosa samples and epithelial cell isolation. Swiss-rolled colon was fixed using 4% PFA. Whole mucosa samples and isolated epithelial cells were snap-frozen using liquid nitrogen and maintained at -80°C.

2.2.5 Histopathological Scoring of the Colonic Sections

H&E-stained colonic sections were assessed using the Histological Activity Index (Table 6) (Laroui et al., 2012). The scoring was done considering 3 parameters: the severity of the inflammation was scored with the lowest score 0 and the highest score 3; the crypt damage was scored with the lowest score 0 and the highest score 5; and the ulceration was scored with the lowest score 0 and the highest score 3. For the final score, the scores coming from these 3 parameters were added to obtain the minimum score of 0 and the maximum score of 11.

Table 6: Histological Activity Index used in the scoring of the H&E-stained colonic sections

Score	Severity of Inflammation	Crypt Damage	Ulceration
0	Rare inflammatory cells in lamina propria	Intact crypts	Absence of ulcer
1	Increased number of granulocytes in the lamina propria	Loss of the basal one-third	1 or 2 foci of ulcerations
2	Confluence of inflammatory cells extending into the submucosa	Loss of the basal two-thirds	3 or 4 foci of ulcerations
3	Transmural extension of the inflammatory infiltrate	Entire crypt loss	Confluent of extensive ulceration
4	-	Change of the epithelial surface with erosion	
5	-	Confluent erosion	

2.2.6 Protein Extraction from Whole Mucosa Samples

1x Tissue Lysis Buffer was added directly onto the frozen tissue samples, followed by homogenization of the tissue by Eppendorf micropestles. Homogenized tissue was

incubated in ice for 10 minutes, then centrifuged at 20,000g for 30 minutes at +4°C. The supernatant, which contains proteins, was collected after the centrifugation and maintained at -80°C.

2.2.7 Protein Quantification

Pierce BCA protein assay kit (Thermo Scientific) was used to quantify the concentration of protein samples. To prepare standards, 2 mg/mL BSA protein solution was first diluted to 100 µg/mL with ddH2O, which was later used to prepare standard protein solution at different concentrations. The final concentrations of the standard protein solutions are as follows in increasing order: 0 µg/mL, 10 µg/mL, 20 µg/mL, 30 µg/mL, 40 µg/mL, 50 µg/mL, 70 µg/mL, and 100 µg/mL. The protein samples were diluted with ddH2O 100 times (4µL protein sample+ 396 µL ddH2O). 100 µL of each standard and protein sample was loaded into a clear, flat-bottomed 96-well plate as triplicates. BCA working reagent was prepared according to the manufacturer's instructions (50 parts of Reagent A+ 1 part of Reagent B). 100 µL of working reagent was added on top of each well. The plate was incubated at 60°C for 50 minutes. The absorbance values were measured at 562nm using Synergy HT Microplate Reader (Biotek). The protein concentration of samples was calculated by using the standard curve created based on the protein concentration and absorbance values of the standards.

2.2.8 Mouse Cytokine Array Kit

In this experiment, Mouse Inflammation Antibody Array C1 (RayBiotech) was used. As the initial step, the membranes were blocked using the Blocking Buffer of the kit at room temperature for 30 minutes. The samples, quantified with the BCA method, were diluted with the blocking buffer to obtain the same amount of protein in a total of 1 mL volume. After the blocking, the Blocking Buffer was removed, and samples were added. The membranes were incubated in the sample solution overnight at +4°C. After the incubation, the membranes were washed as instructed by the provider. Then, 1 mL of Biotinylated Antibody Cocktail was added to each membrane and incubated for 2 hours at room temperature. The membranes were washed and incubated in 2 mL

of 1x HRP-Streptavidin for 2 hours at room temperature. After the excess HRP-Streptavidin was washed, membranes were incubated in the Detection Buffer for 2 minutes at room temperature. Then, the chemiluminescent signals were detected with Amersham Imager 600. The detected signals were analyzed and normalized as instructed by the provider.

2.2.9 Oxidative Stress Analysis Kits

For Total Superoxide Dismutase activity analysis, the Total Superoxide Dismutase (T-SOD) Activity Assay Kit (WST-1 Method) (Elabscience) was used.

For Glutathione Peroxidase activity analysis, the Glutathione Peroxidase (GSH-Px) Activity Assay Kit (Elabscience) was used.

For Catalase activity analysis, the Catalase (CAT) Activity Assay Kit (Elabscience) was used.

For Malondialdehyde analysis, the Malondialdehyde (MDA) Colorimetric Assay Kit (TBA Method) (Elabscience) was used.

Each kit was performed according to the manufacturer's instructions.

2.2.10 RNA Isolation

RNA was isolated from whole mucosa samples using TRIpure Total RNA Extraction Reagent (ELK Biotechnology). 1 mL TRIpure reagent was added directly onto the frozen samples, which were then homogenized with Eppendorf micropestles. Homogenized samples were incubated at room temperature for 5 minutes. The samples were shaken vigorously for 15 seconds after adding 300 µL chloroform, followed by a 3-minute incubation at room temperature. After the incubation, the samples were centrifuged at 12,000g for 15 minutes at +4°C, which leads to phase separation. The aqueous phase was collected and mixed with isopropanol at the same volume of the collected aqueous phase, which was later followed by a 20-minute incubation at -20°C and centrifugation at 12,000g for 10 minutes at +4°C. The supernatant was removed, and the pellet was washed by adding 1 mL of 75% ethanol onto the pellet, mixing with

a vortex mixer, and centrifuging at 7500g for 5 minutes at +4°C. Later, the air-dried pellet was dissolved in DEP-C treated water by pipetting.

The concentration and the purity of the isolated RNA samples were measured using NanoDrop One (Thermo Scientific). RNA samples were maintained at -80°C.

2.2.11 cDNA Generation and qPCR

cDNA generation was done using PrimeScript RT Master Mix (Takara). RNA samples isolated from the mouse whole mucosa samples were used as the template in each reaction. The reverse-transcription reaction solution was prepared by mixing 500 ng total RNA, 5X PrimeScript RT Master Mix, and RNase-free water. The reverse transcription reaction was performed by incubating the reverse-transcription reaction solution in a thermocycler at the following conditions: 15 minutes at 37°C and 5 seconds at 85°C.

To perform qPCR, LightCycler 480 SYBR Green I Master (Roche) was used. The generated cDNA samples were diluted with nuclease-free water (1:4, cDNA: nuclease-free water), and mixed with SYBR green, 10 µM primer mixture, and nuclease-free water. The reaction mixtures were loaded into 96-well plates and sealed with an optical sealing foil. The reaction was performed at the following conditions:

-Pre-incubation at 95°C for 5 minutes

-Amplification (45 cycles)

-95°C for 10 seconds

-60°C for 10 seconds

-72°C for 10 seconds

Chapter 3

Results

3.1 Inhibition of IKK-Related Kinases Aggravates Inflammatory Phenotype in Acute UC

To generate acute UC models, we treated mice with 3% DSS mixed in drinking water for 5 days. After 5 days, we changed their water back to drinking water without DSS for the recovery period, which lasted 9 days. During the whole experiment, we treated the animals either with Amlexanox (Amlexanox group) or vehicle solution as the control group (Vehicle group). First, we evaluated their inflammation phenotypically. For this evaluation, we considered the clinical scores recorded throughout the experiment, the histological activity index score of the colon, the colon length measured right after the sacrifice, and the change in weight percentage throughout the experiment (Figure 3).

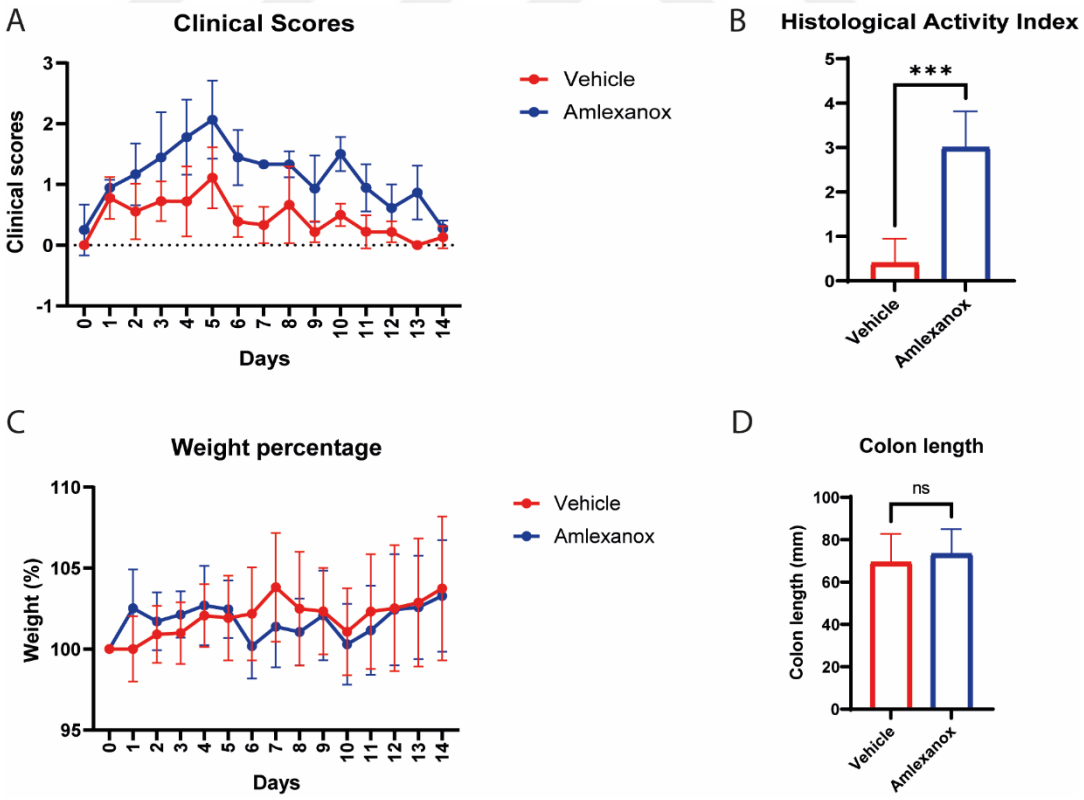

Figure 3: Evaluation of the inflammatory status in acute UC model phenotypically. This evaluation includes **A)** clinical scores that were assigned daily

based on weight loss, fecal consistency, and fecal blood content throughout the experiment, **B)** histological activity index of the colon based on the severity of the inflammation, crypt damage, and ulceration, **C)** weight percentage of the mice throughout the experiment, assigning the weight at the beginning of the experiment as 100%, **D)** length of the colon in millimeters, measured right after the sacrifice

The Amlexanox group showed a higher clinical score than the Vehicle group throughout the experiment (Figure 3A), indicating an elevated level of inflammation. We observed a much higher histological activity index on average for the Amlexanox group than the Vehicle group (Figure 3B), indicating an increased inflammation and tissue damage in the Amlexanox group. When we look at the weight percentage throughout the experiment (Figure 3C), we observe that the weight of the Amlexanox group got worse than the Vehicle group later in the experiment, although at the beginning of the DSS treatment, their weight increased more than the Vehicle group This indicates a worsened health status in the Amlexanox group after the induction of the inflammation. The length of the colon is known to decrease upon inflammation. Therefore, colon length can be used as an indirect measure to evaluate the inflammatory status (Kang et al., 2021). However, in this experiment, we did not observe any meaningful change in the colon length (Figure 3D).

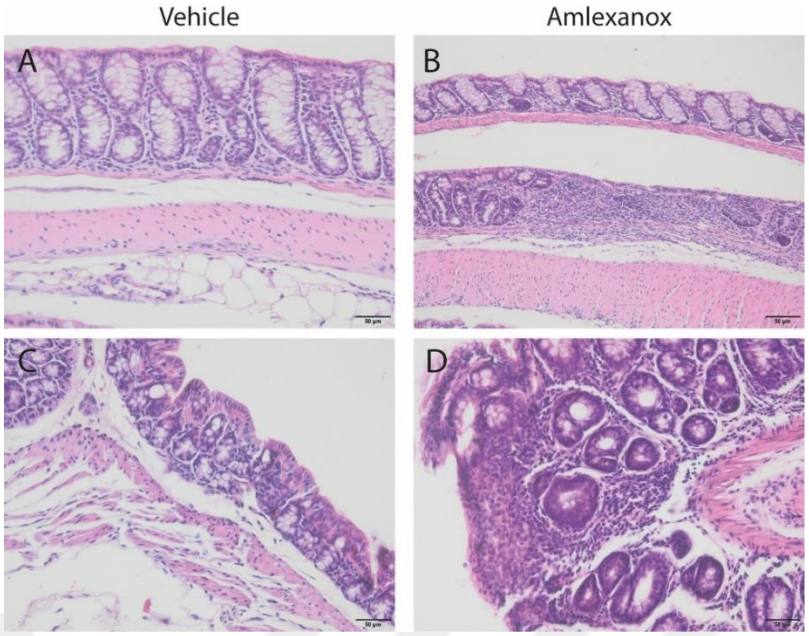

Figure 4: Hematoxylin and eosin (H&E) staining of the colon of acute UC mice. Pictures show the H&E-stained colon of two mice from each group. The scale bar represents 50µm.

With H&E staining of the mouse colons, elevated tissue damage can be observed in the Amlexanox group (Figure 4). The stained tissue of the Amlexanox group (Figure 4B&D) shows abruptions in the crypt structure, indicating tissue damage, while the stained tissue of the Vehicle group (Figure 4A&C) shows regular crypt structures.

3.2 Inhibition of IKK-Related Kinases Changes the Cytokine Profile in Acute UC

To investigate the changes in the cytokine levels in the mouse colon due to acute UC, we analyzed the colon whole mucosa protein samples using the Mouse Inflammation Array (RayBiotech), which can detect the level of 40 different cytokines simultaneously.

In that analysis, we detected a change in the expression level of 8 cytokines (Figure 5). Among these 8 cytokines, only 3 of them, which are CCL11 (Eotaxin-1), CCL24 (Eotaxin-2), and CX3CL1 (Fractalkine), show a statistically significant increase upon Amlexanox treatment. In addition to those, FasL and IL10 levels display an increase upon Amlexanox treatment, although it is not statistically significant. Moreover, we observed a decrease in the expression level of CCL25 (TECK), soluble TNFα

Receptor-I (sTNF RI), and soluble TNFα Receptor-II (sTNF RII) in the Amlexanox group, although those are not statistically significant either.

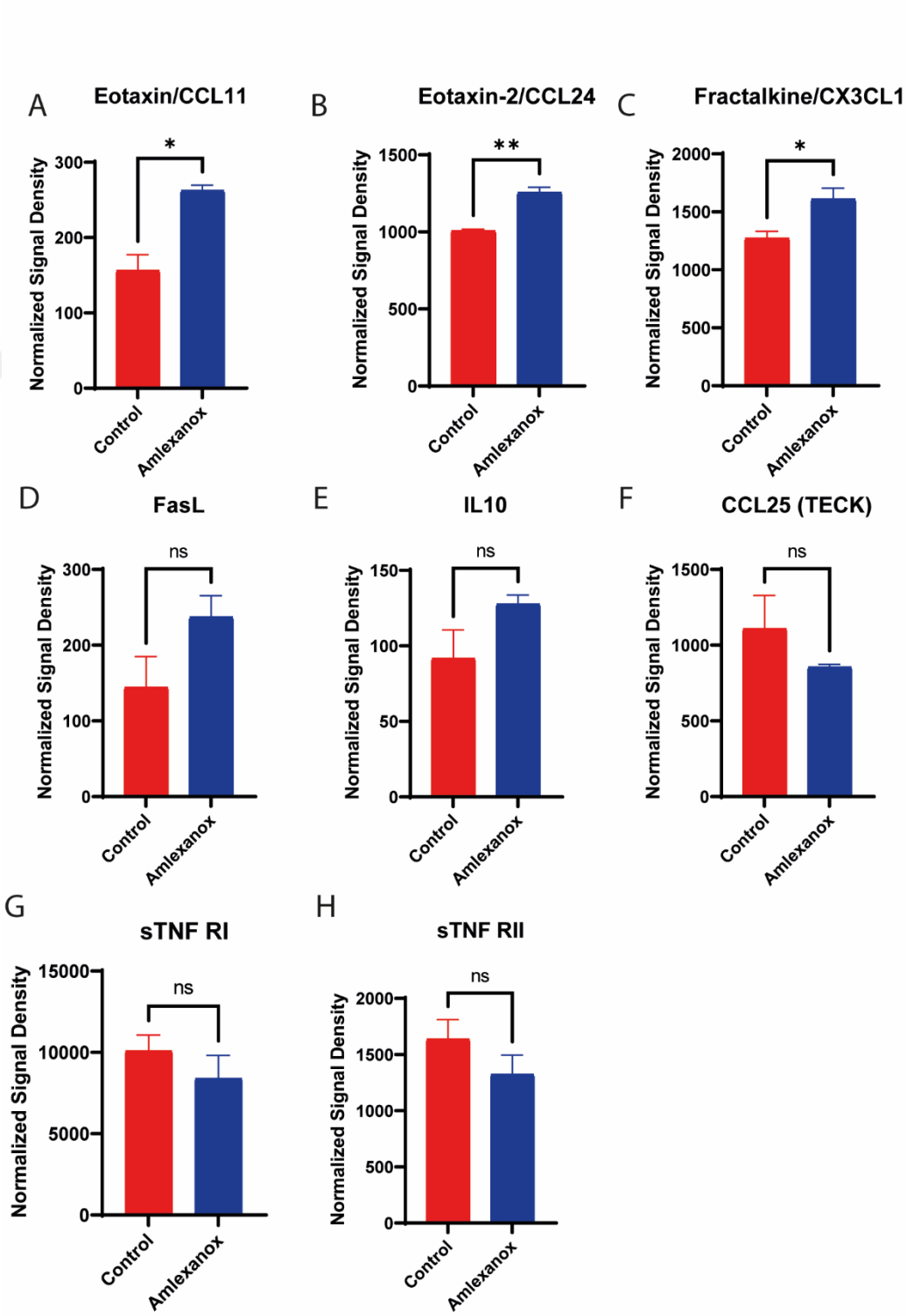

Figure 5: Mouse Cytokine Array results of the acute UC experiment. Protein samples extracted from the whole mucosa of 2 mice/group were analyzed.

To further analyze the change in the expression level of cytokines in acute UC, we performed qPCR using the RNA samples extracted from colonic whole mucosa samples of acute UC (Figure 6).

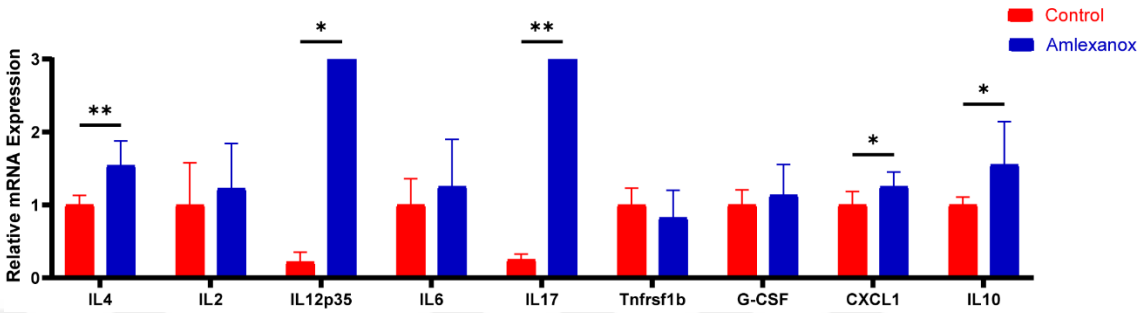

Figure 6:mRNA expression level of selected cytokines in acute UC experiment. Total RNA samples extracted from the colonic mucosa of 3 mice/group were used for qPCR.

We observed a statistically significant increase in the mRNA expression levels of proinflammatory cytokines IL-4, IL-12, IL-17, and chemokine CXCL1. We observed a tendency for an increase in the mRNA expression levels of proinflammatory cytokines IL-2, IL-6, and G-CSF in the Amlexanox group, although the change in their expression level is not statistically meaningful. We observed a statistically significant increase in the mRNA expression level of anti-inflammatory cytokine IL-10 in the Amlexanox group, supporting the Mouse Cytokine Array result. Additionally, the mRNA level of Tnfrf1b, which encodes the TNF RII protein, displays a non-significant decrease in the Amlexanox group, which also shows the same pattern as the Mouse Cytokine Array result.

3.3 Inhibition of IKK-Related Kinases Changes the Infiltrated Immune Cell Profile in Acute UC

To assess the immune cell infiltration in the colonic microenvironment of acute UC model animals, we checked specific immune cell markers by utilizing qPCR (Figure 7). For this analysis, we used the same RNA samples as in the qPCR experiments, in which we checked the cytokine profile.

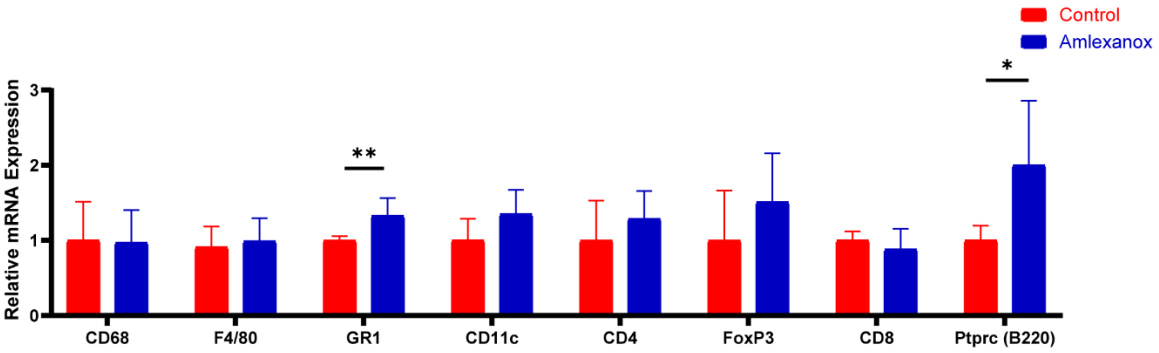

Figure 7: mRNA expression level of immune cell markers in acute UC experiment. Total RNA samples extracted from the colonic mucosa of 3 mice/group were used for qPCR.

The qPCR result shows no significant change in the mRNA expression levels of CD68 and F4/80, which are monocyte and macrophage markers, respectively. On the other hand, the mRNA expression level of the granulocyte marker GR1 shows a statistically significant increase, while the dendritic cell marker CD11c shows a non-significant increase in the Amlexanox group. Taken together, these data indicate an increased innate immune cell infiltration to the colon in the acute UC model upon Amlexanox treatment. The mRNA level of the helper T-cell marker CD4 and Treg marker FoxP3 show a non-significant increase, while the cytotoxic T-cell marker CD8 does not show a meaningful change. Therefore, it can be speculated that in this model, IKK-related kinase inhibition does not cause a detrimental change in the T-cell infiltration to the colon. However, the mRNA level of B-cell marker B220 shows an approximately 2-fold increase, indicating increased B-cell infiltration to the colon upon inhibition of the IKK-related kinases.

Although we did not see any meaningful change in the total macrophage level, we performed another qPCR targeting the expression level of M1 macrophage and M2 macrophage markers to gain a better insight into macrophage response in this model (Figure 8).

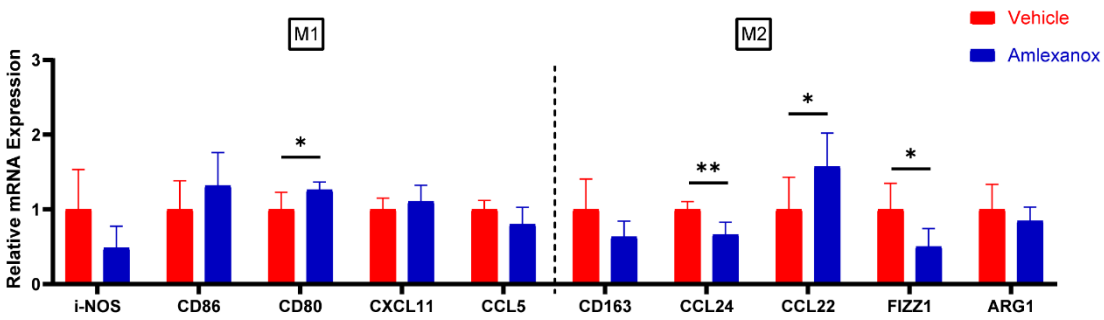

Figure 8: mRNA expression level of macrophage polarization markers in acute UC experiment. Total RNA samples extracted from the colonic mucosa of 3 mice/group were used for qPCR.

Among the M1-polarization markers, the mRNA level of CD80 shows a statistically significant increase; the mRNA levels of CD86 and CXCL11 show a non-significant increase, while the mRNA levels of i-NOS and CCL5 show a non-significant decrease. All M2-polarization markers checked show a decrease. mRNA levels of CCL24, CCL22, and FIZZ1 show a significant decrease, and the mRNA levels of CD163 and ARG1 show a non-significant decrease. Taken together, the change in the mRNA expression levels of these markers shows a shift towards a more M1-like macrophage response upon Amlexanox treatment, although there is no clear-cut shift in macrophage polarization. Therefore, we can speculate that although total macrophage infiltration does not show a meaningful change, its polarization shifts toward a more proinflammatory response in the acute UC model upon inhibition of IKK-related kinases.

3.4 Inhibition of IKK-Related Kinases Cause an Impairment in the Antioxidant Metabolism in Acute UC

As a further evaluation of the inflammatory status of the colon upon Amlexanox treatment during acute UC, we assessed the oxidative stress status using colorimetric kits. In this regard, we checked the enzymatic activity of antioxidant enzymes total superoxide dismutase (T-SOD), catalase (CAT), and glutathione peroxidase (GSH-Px). Additionally, we checked the concentration of lipid oxidation byproduct malondialdehyde (MDA) (Figure 9).

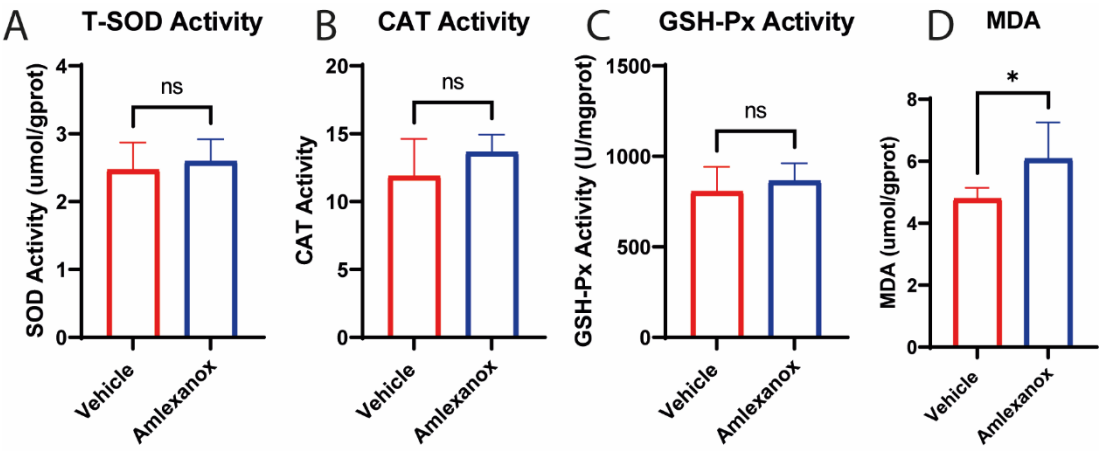

Figure 9: Oxidative stress markers in acute UC. Total protein samples extracted from colonic whole mucosa were analyzed using colorimetric assays.

The activity levels of the antioxidant enzymes checked do not show any meaningful change in the Amlexanox group. MDA concentration, on the other hand, showed a significant increase in the Amlexanox group. Not seeing any change in the antioxidant enzyme activity levels was unexpected since we observed an increase in the inflammatory response in the previous experiments. Therefore, we decided to check the activity of the NRF2, the "master regulator" of antioxidant response. For this purpose, we checked the mRNA expression levels of NRF2 target genes, whose transcription is directly controlled by NRF2 (Figure 10).

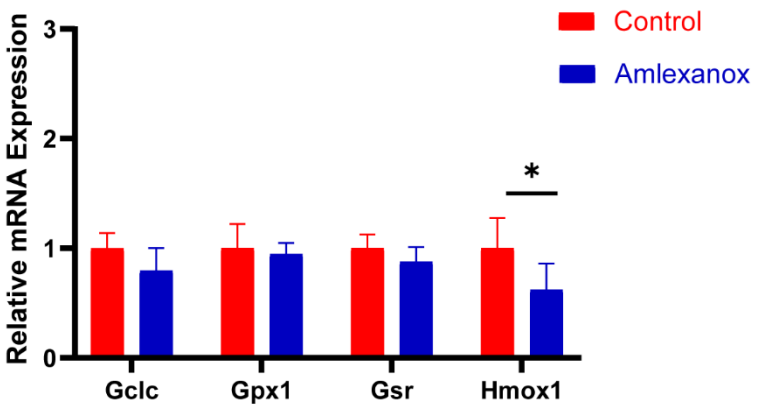

Figure 10: mRNA expression levels of NRF2 target genes in acute UC model. Total RNA samples extracted from the colonic mucosa of 3 mice/group were used for qPCR.

We checked four NRF2 target genes, which are Gclc, Gpx1, Gsr, and Hmox1. We observed a decrease in the mRNA expression level of Hmox1 and did not observe a meaningful change in the mRNA expression levels of the other NRF2-target genes, including Gclc, Gpx1, and Gsr. Overall, NRF2 activity does not seem to be fully functional in the acute UC model when IKK-related kinases are inhibited.

3.5 Inhibition of IKK-Related Kinases Aggravates Inflammatory Phenotype in Chronic UC

To generate chronic UC model, we treated mice with DSS in drinking water for 3 cycles. Each cycle contains 5 days of DSS treatment and 9 days of recovery period, where we change the water back to the regular drinking water. We used 3% DSS in the first cycle, 2.75% DSS in the second cycle, and 2.25% DSS in the third cycle. During the whole experiment, we treated the animals either with Amlexanox (Amlexanox group) or vehicle solution as the control group (Vehicle group). Similar to the acute UC model, we evaluated the inflammatory level phenotypically as the initial step of the study. For this evaluation, we considered the clinical scores recorded throughout the experiment, the histological activity index score of the colon, the weight change throughout the experiment, and the colon length measured right after the sacrifice (Figure 11).

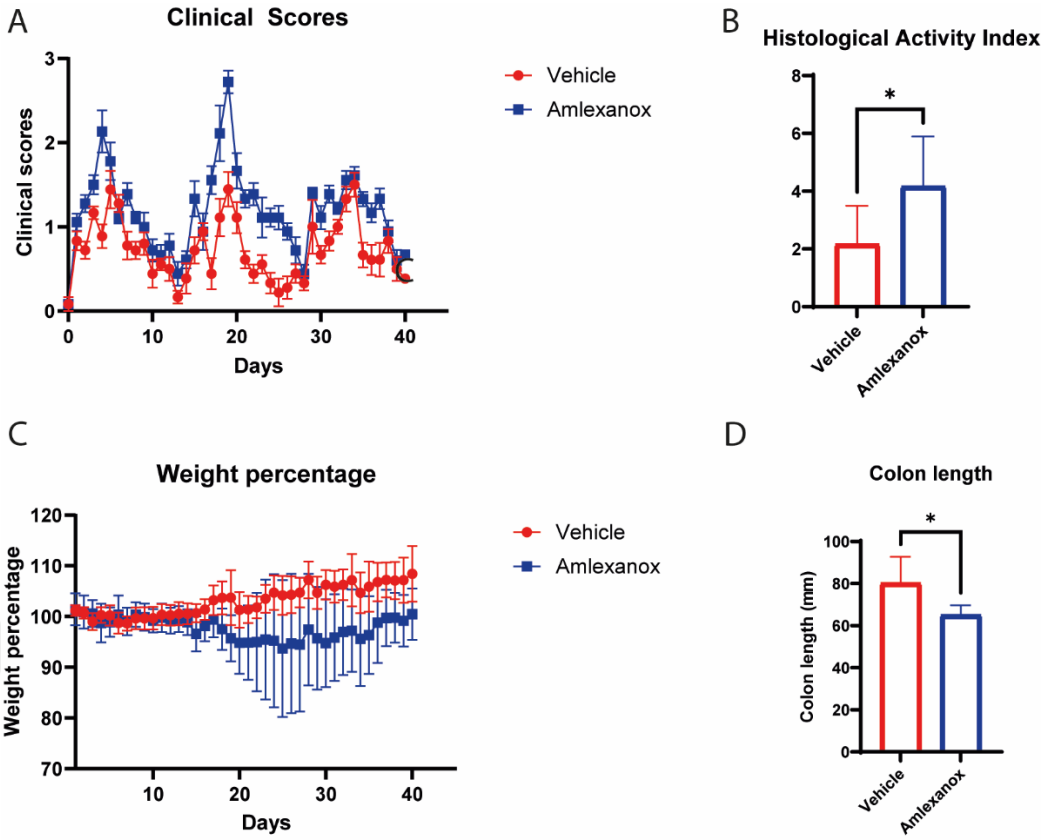

Figure 11: Evaluation of the inflammatory status in chronic UC model phenotypically. This evaluation includes **A)** clinical scores that were assigned daily based on weight loss, fecal consistency, and fecal blood content throughout the experiment, **B)** histological activity index of the colon based on the severity of the inflammation, crypt damage, and ulceration, **C)** weight percentage of the mice throughout the experiment, assigning the weight at the beginning of the experiment as 100%, **D)** length of the colon in millimeters, measured right after the sacrifice

The clinical score of the Amlexanox group was higher than that of the Vehicle group throughout the experiment (Figure 11A), which indicates an elevated level of inflammation. The Amlexanox group also showed a significantly higher histological activity index (Figure 11B), which indicates elevated inflammation and tissue damage. When we look at the weight percentage throughout the experiment (Figure 11C), we see that although the two groups show a similar average weight percentage at the beginning of the DSS treatment, the Amlexanox group started to lose weight while the Vehicle group was gaining weight later in the DSS cycle. This indicates a worsened health status in the Amlexanox group, especially after the second DSS cycle beginned,

preventing them from recovering even during the recovery periods. The average colon length of the Amlexanox group was significantly lower than that of the Vehicle group (Figure 11D), which can also be considered an indication of increased inflammatory phenotype in the Amlexanox group.

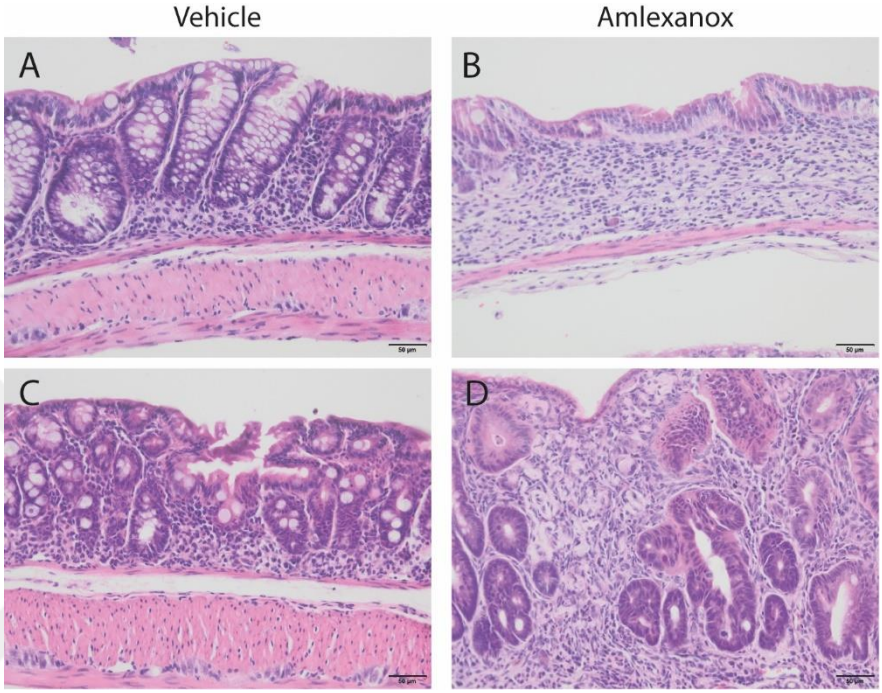

Figure 12: Hematoxylin and eosin (H&E) staining of the colon of chronic UC mice. Pictures show the H&E-stained colon of two mice from each group. The scale bar represents 50µm.

With H&E staining of the mouse colons, significant tissue damage can be observed in the Amlexanox group (Figure 12). While the Vehicle group (Figures 12A&C) still contains visible crypt structures, the visible crypt structures of the Amlexanox group (Figures 12B&D) remain highly limited.

3.6 Inhibition of IKK-Related Kinases Changes the Cytokine Profile in Chronic UC

To evaluate the effect of Amlexanox treatment on the cytokine profile during chronic UC, we analyzed the colon whole mucosa protein samples using the Mouse

Inflammation Array (RayBiotech), which can detect the level of 40 different cytokines simultaneously.

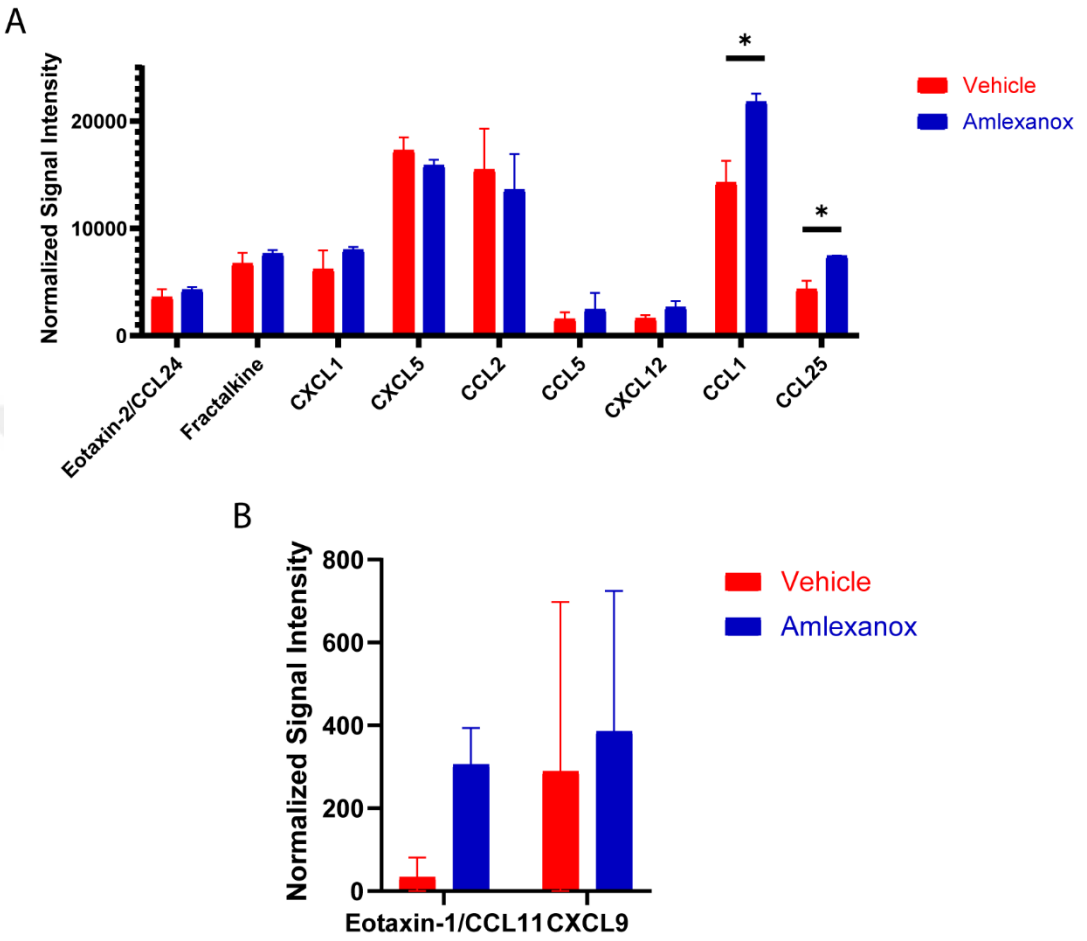

Figure 13: Chemokine profile of chronic UC experiment based on Mouse Cytokine Array results. Protein samples extracted from the whole mucosa of 2 mice/group were analyzed.

In this analysis, we detected changes in the protein level of numerous chemokines (Figure 13). Among these, CCL1 and CCL25 show a statistically significant increase in the Amlexanox group. In addition, the protein levels of Eotaxin-2, Fractalkine, CXCL1, Eotaxine-1, and CXCL9 show a non-significant increase. On the other hand, protein levels of CXCL5 and CCL2 show a non-significant decrease. In general, the protein levels of chemokines show an increase in the Amlexanox group, which might promote immune cell infiltration to the colon.

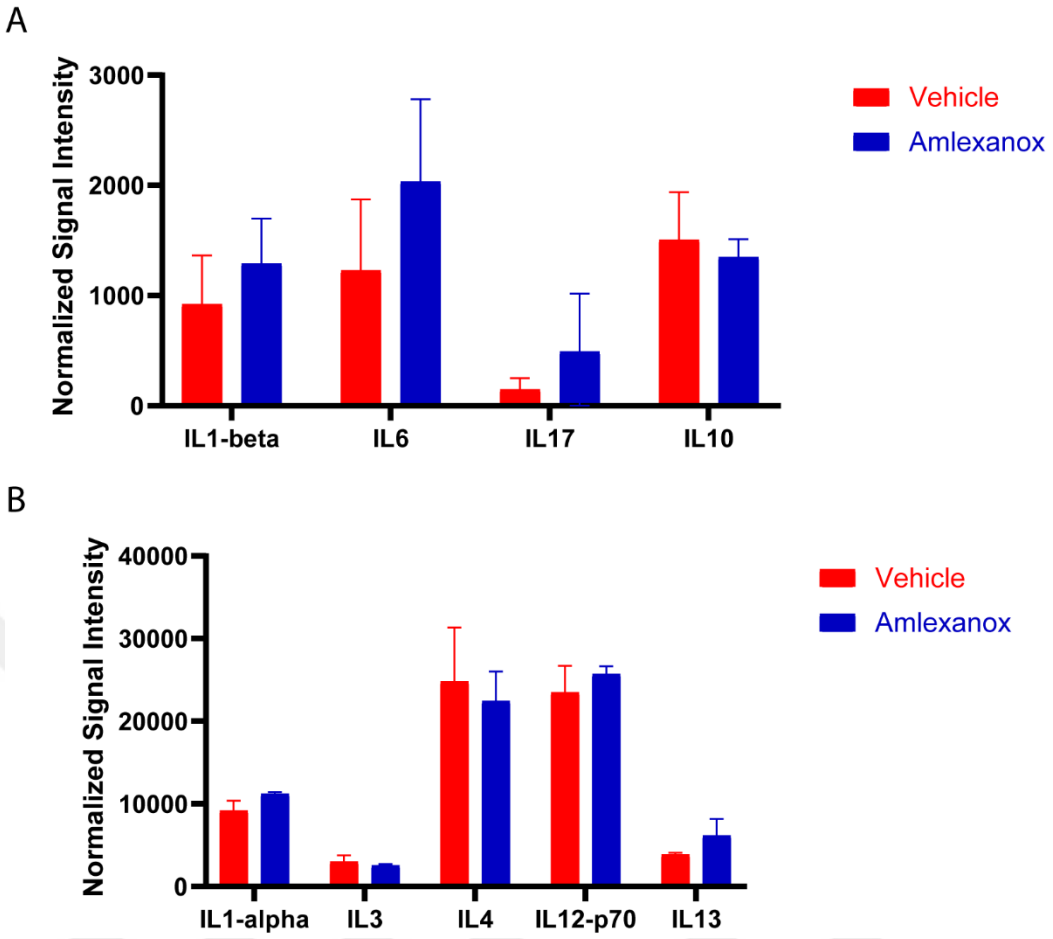

Figure 14: Interleukin expression profile of chronic UC experiment based on Mouse Cytokine Array results. Protein samples extracted from the whole mucosa of 2 mice/group were analyzed.

Furthermore, we detected changes in the expression level of various interleukins in the chronic UC model upon Amlexanox treatment, although none of those changes possess statistical significance (Figure 14). We observed increase in the protein levels of proinflammatory cytokines IL-1β, IL-6, IL-17, IL-1α, and IL-12. The protein level of the anti-inflammatory cytokine IL-10 showed a slight decrease, while the protein level of the anti-inflammatory cytokine IL-3 showed a slight increase. Protein levels of pro-inflammatory cytokines IL-3 and IL-4 also showed a slight decrease.

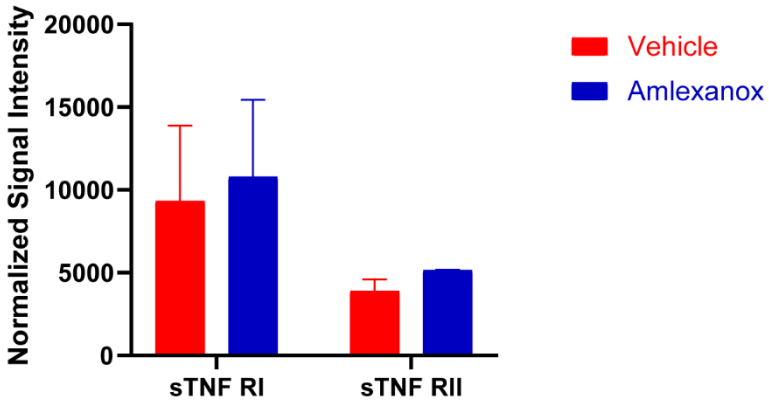

Figure 15: Levels of soluble TNF-α receptors in chronic UC experiment based on Mouse Cytokine Array results. Protein samples extracted from the whole mucosa of 2 mice/group were analyzed.

Additionally, the results of the Mouse Cytokine Array showed an increase in the protein levels of soluble TNF-α receptors in the chronic UC model upon Amlexanox treatment (Figure 15).

To analyze the change in the expression level of cytokines further in chronic UC, we performed qPCR with the RNA samples extracted from colonic whole mucosa samples of the chronic UC experiment (Figure 16).

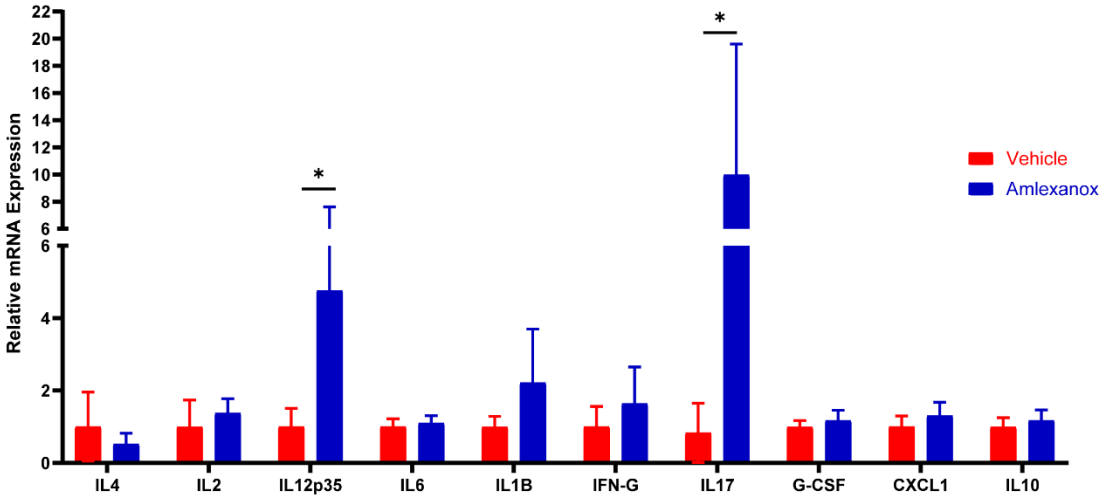

Figure 16:mRNA expression level of selected cytokines in chronic UC experiment. Total RNA samples extracted from the colonic mucosa of 3 mice/group were used for qPCR.

We observed a statistically significant increase in the mRNA expression levels of proinflammatory cytokines IL-12 and IL-17 in the Amlexanox group. Moreover, we observed a non-significant change in the mRNA expression levels of pro-inflammatory cytokines IL-2, IL-1β, IFN-γ, and CXCL1. Interestingly, the mRNA expression level of the pro-inflammatory cytokine IL-4 showed a non-significant decrease in the Amlexanox group.

3.7 Inhibition of IKK-Related Kinases Changes the Infiltrated Immune Cell Profile in Chronic UC

We analyzed the immune cell markers with qPCR to evaluate the immune cell infiltration in the colon of chronic UC model animals (Figure 17). For this analysis, we used the same RNA samples as in the qPCR experiments, in which we checked the cytokine profile.

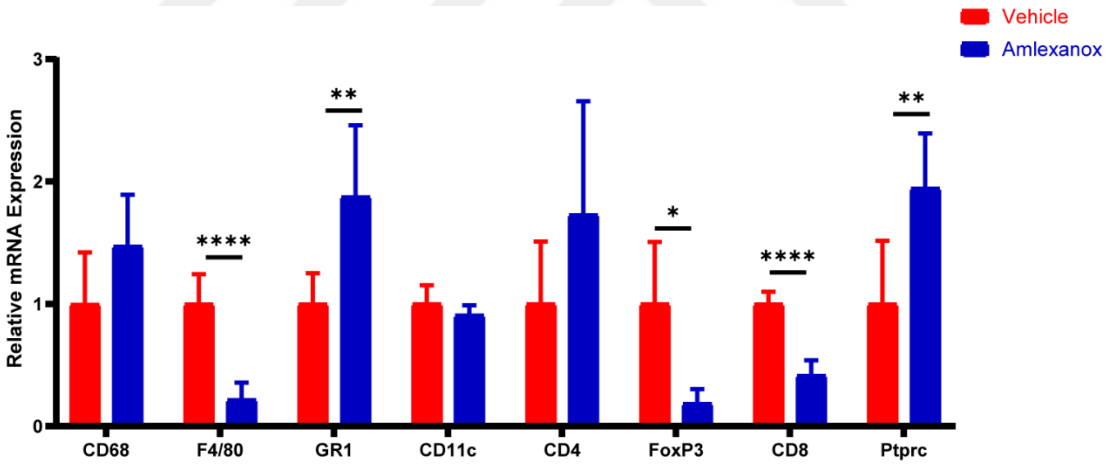

Figure 17: mRNA expression level of immune cell markers in the chronic UC experiment. Total RNA samples extracted from the colonic mucosa of 3 mice/group were used for qPCR.

The qPCR result shows a non-significant increase in the mRNA expression level of monocyte marker CD68 and a significant increase in the granulocyte marker GR1 in the Amlexanox group, suggesting increased monocyte and granulocyte infiltration. The mRNA expression level of macrophage marker F4/80, on the other hand, shows a

highly significant decrease in the Amlexanox group. The mRNA expression level of helper T-cell marker CD4 shows a non-significant increase in the Amlexanox group. In contrast, mRNA expression of level cytotoxic T-cell marker CD8 and Treg marker FoxP3 show a statistically significant decrease. Similar to acute UC results, B-cell marker B220 shows an almost 2-fold increase in the mRNA expression level upon Amlexanox treatment. These data show an increased infiltration of adaptive immune cells to the colon during chronic UC upon Amlexanox treatment, indicating an elevated adaptive immune response.

We analyzed the same samples with qPCR targeting the expression levels of M1 macrophage and M2 macrophage markers to gain a better insight into macrophage response in this model (Figure 18).

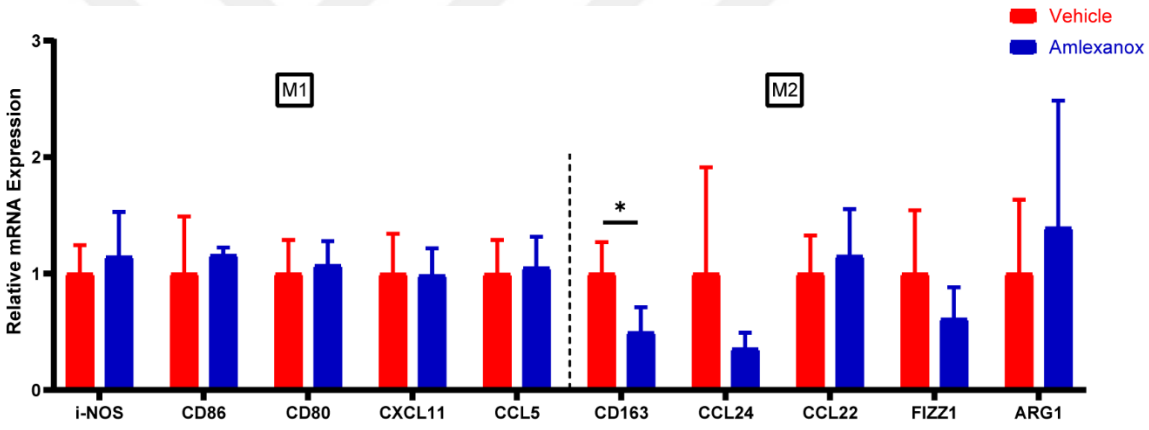

Figure 18: mRNA expression level of macrophage polarization markers in the chronic UC experiment. Total RNA samples extracted from the colonic mucosa of 3 mice/group were used for qPCR.

The mRNA expression level of M1-polarization markers does not show a significant change upon Amlexanox treatment in chronic UC, although they show a slight tendency to increase. Among the M2-polarization markers, CD163 shows a significant decrease. Additionally, mRNA expression levels of CCL24 and FIZZ1 show a non-significant decrease, while mRNA expression levels of CCL22 and ARG1 show a non-significant increase in the Amlexanox group. This data can be interpreted as slightly shifting toward a more M1-like macrophage response upon Amlexanox treatment. Therefore, although total macrophage infiltration in the Amlexanox group drops in the

chronic UC model, the macrophage profile shows an incline toward a proinflammatory response.

3.8 Inhibition of IKK-Related Kinases Cause an Impairment in the Antioxidant Metabolism in Chronic UC

To further evaluate the inflammatory status of the colon during chronic UC upon Amlexanox treatment, we utilized colorimetric oxidative stress kits. For this purpose, we checked the enzymatic activity of antioxidant enzymes total superoxide dismutase (T-SOD), catalase (CAT), and glutathione peroxidase (GSH-Px). Additionally, we checked the concentration of lipid oxidation byproduct malondialdehyde (MDA) (Figure 19).

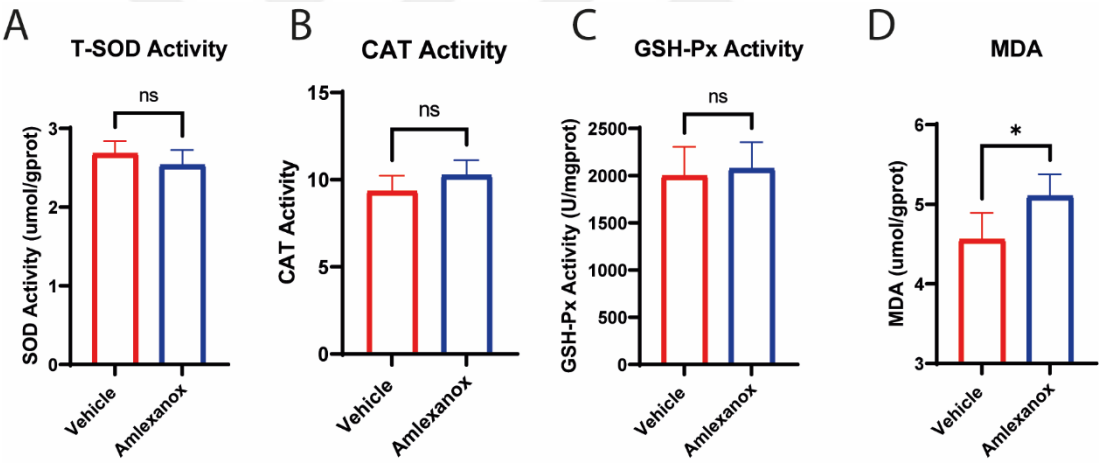

Figure 19: Oxidative stress markers in the chronic UC experiment. Total protein samples extracted from colonic whole mucosa were analyzed using colorimetric assays.

Similar to the acute UC experiment, the activity levels of the antioxidant enzymes checked do not show any meaningful change in the Amlexanox group. However, MDA concentration shows a significant increase in the Amlexanox group. Since we did not see any change in the antioxidant enzyme activity level, we wanted to check the NRF2 activity, similar to the acute UC experiment. Again, for this purpose, we checked the

mRNA expression levels of NRF2 target genes, whose transcription is directly controlled by NRF2 (Figure 20).

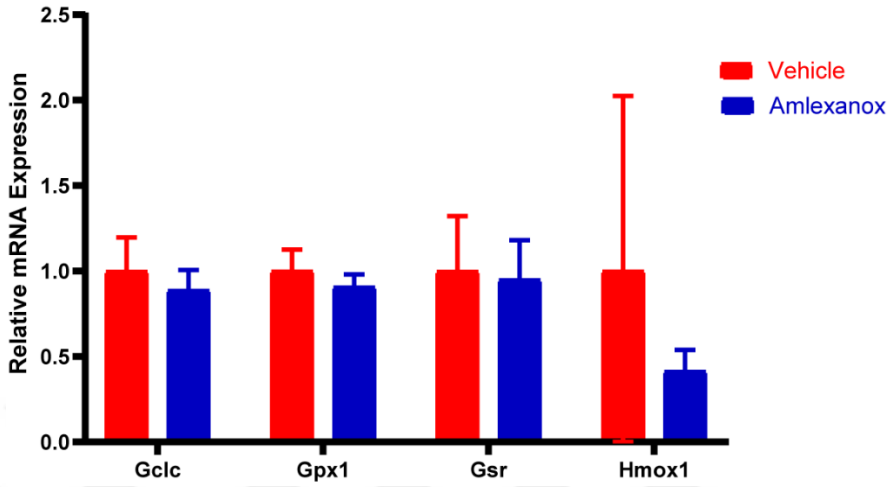

Figure 20: mRNA expression levels of NRF2 target genes in the chronic UC model. Total RNA samples extracted from the colonic mucosa of 3 mice/group were used for qPCR.

We checked the mRNA expression levels of four NRF2 target genes: Gclc, Gpx1, Gsr, and Hmox1. We did not observe any meaningful change in the mRNA expression levels of the NRF2-target genes that we checked.

Chapter 4

Discussion

UC is an inflammatory condition mainly resulting from the disruption of the immunological balance in the colon. Although the exact pathophysiology of the UC is not completely uncovered, the major factors contributing to it are disruption of the intestinal barrier, problems with the resolution of the immune response, and abruptions in the tolerance mechanisms to the microbiota (Saez et al., 2023). IKK-related kinases play crucial roles in different pathways modulating immune activity. In this study, we aimed to uncover the role of IKK-related kinases on UC at different phases of the disease (Häcker & Karin, 2006; Llona-Minguez et al., 2013).

For this purpose, we used DSS-induced colitis mouse models with FVB/N mice. We treated mice with Amlexanox, a dual inhibitor of the IKK-related kinases, during the whole experiment. Moreover, to understand the role of IKK-related kinases at different stages of the disease, we used acute and chronic models of DSS-induced colitis.

In these models, our physiological observations, including clinical and histopathological scores, indicated increased inflammation upon inhibition of the IKK-related kinases in both acute and chronic models. We performed various biochemical analyses, such as qPCR, Mouse Cytokine Array, and oxidative stress assays, using the tissue samples collected from model animals.

When we analyzed samples from both experiments with the Mouse Cytokine Array, we observed a striking difference in the number of cytokines that showed change between the groups. For acute UC samples, we observed a meaningful change in the protein level of only a few cytokines. For chronic UC samples, on the other hand, we observed a meaningful change in the protein level of more than half of the cytokines included in the kit, although not all were statistically significant. This indicates that IKK-related kinases affect inflammatory response in UC more elaborately at the chronic phase than at the onset of the disease. An increase in the protein levels of different chemokines was observed in both phases, which would cause elevated infiltration of different immune cells, supporting our initial observation about increased inflammatory response. In both experiments, we observed an increase in Eotaxin-1 and Eotaxin-2 levels, which act as eosinophil chemoattractants (Huber et

al., 2018). When we analyzed immune cell markers with qPCR, we observed a significant increase in the mRNA level of the granulocyte marker GR1, showing an increase in granulocyte recruitment, which is likely to include eosinophils.

In both phases, we observe an increase in the mRNA expression level of proinflammatory cytokines in the Amlexanox group. However, the cytokines that show an increase are not identical. This might be attributed to having different types of immune cells in the microenvironment during different stages of the inflammation. Interestingly, in the acute phase, the mRNA level of anti-inflammatory cytokine IL-10 shows a significant increase in the Amlexanox group, while its change is not meaningful in the chronic phase. This might be explained by the increase of Treg cells in the Amlexanox group in the acute phase (although it is not statistically significant), and their significant decrease in the chronic phase.

The profile of immune cell markers shows some important distinctions between the two phases. In the acute phase, innate immune cell markers show an increase in the Amlexanox group in general, while the helper T-cell marker CD4, which is crucial for adaptive immune response, does not show a meaningful change. In the chronic phase, however, innate immune cell markers do not show much increase in the Amlexanox group, while CD4 increases. Interestingly, in both phases, the cytotoxic T-cell marker CD8 shows a decrease, non-significant in the acute phase and significant in the chronic phase. It indicates a lowered cytotoxicity in the microenvironment, which might be subject for further investigation in the project. In both acute and chronic phases, B-cell marker B220 show a significant increase, indicating elevated humoral response upon inhibition of IKK-related kinases.

Overall, we observe an increase in the inflammatory response and tissue damage in the Amlexanox group, which indicates increased oxidative stress and, thus, increased ROS production. Normally, it is expected to see increased antioxidant enzyme activity levels upon elevated ROS, trying to protect the tissue. However, when we analyzed the antioxidant enzyme levels of our samples, we did not observe any meaningful change. Moreover, we observed an increased concentration of MDA, which indicates increased oxidation. We hypothesized it might be related to some impairment in the activity of the "master regulator" of antioxidant response NRF2. To test our hypothesis, we analyzed the mRNA expression levels of some of the transcriptional

targets of NRF2. Normally, the activity of NRF2 increases under inflammatory conditions, which causes the upregulation of its target proteins (He et al., 2020). However, when we checked the mRNA expression levels of NRF-target genes, we observed either a decrease or no change in the Amlexanox group in both acute and chronic UC models. This finding indicates an impairment of NRF2 activity when the IKK-related kinases are inhibited.

Taking all of these data together, we hypothesize that IKK-related kinases might play an important role in NRF2 activity. Inhibition of their activity might be impairing NRF2 activity, leading to increased oxidative stress, which causes tissue damage creating an elevated inflammatory response in ulcerative colitis.

In our study, we observed the collective role of IKKε and TBK1 due to using a dual kinase inhibitor. However, they may play different roles individually. To be able to understand their individual roles on UC, engineered mouse models with only one of these genes knocked-out can be utilized for further investigation.

REFERENCES

Alshehri, D., Saadah, O., Mosli, M., Edris, S., Alhindi, R., & Bahieldin, A. (2021). Dysbiosis of gut microbiota in inflammatory bowel disease: Current therapies and potential for microbiota-modulating therapeutic approaches. In *Bosnian journal of basic medical sciences* (Vol. 21, Issue 3, pp. 270–283). NLM (Medline). https://doi.org/10.17305/bjbms.2020.5016

Attri, S., Bansal, S., & Goel, G. (2022). An introduction to human gut microbiome. In *Human-Gut Microbiome: Establishment and Interactions* (pp. 3–14). Elsevier. https://doi.org/10.1016/B978-0-323-91313-3.00014-3

Azuma, Y. T., Hagi, K., Shintani, N., Kuwamura, M., Nakajima, H., Hashimoto, H., Baba, A., & Takeuchi, T. (2008). PACAP provides colonic protection against dextran sodium sulfate induced colitis. *Journal of Cellular Physiology*, *216*(1), 111–119. https://doi.org/10.1002/JCP.21381

Azzouz, L. L., & Sharma, S. (2023). *Physiology, Large Intestine*. StatPearls Publishing, Treasure Island (FL). http://europepmc.org/abstract/MED/29939634

Bellezza, I., Giambanco, I., Minelli, A., & Donato, R. (2018). Nrf2-Keap1 signaling in oxidative and reductive stress. *Biochimica et Biophysica Acta (BBA) - Molecular Cell Research*, *1865*(5), 721–733. https://doi.org/10.1016/J.BBAMCR.2018.02.010

Blanco, A., & Blanco, G. (2022). Antioxidants. *Medical Biochemistry*, 221–231. https://doi.org/10.1016/B978-0-323-91599-1.00007-9

Bonilla, F. A., & Oettgen, H. C. (2010). Adaptive immunity. *Journal of Allergy and Clinical Immunology*, *125*(2 SUPPL. 2). https://doi.org/10.1016/j.jaci.2009.09.017

Clément, J. F., Meloche, S., & Servant, M. J. (2008). The IKK-related kinases: from innate immunity to oncogenesis. *Cell Research 2008 18:9*, *18*(9), 889–899. https://doi.org/10.1038/cr.2008.273

Geremia, A., Biancheri, P., Allan, P., Corazza, G. R., & Di Sabatino, A. (2014). Innate and adaptive immunity in inflammatory bowel disease. In *Autoimmunity Reviews* (Vol. 13, Issue 1, pp. 3–10). https://doi.org/10.1016/j.autrev.2013.06.004

Gribble, F. M., & Reimann, F. (2019). Function and mechanisms of enteroendocrine cells and gut hormones in metabolism. *Nature Reviews Endocrinology*, *15*(4), 226–237. https://doi.org/10.1038/s41574-019-0168-8

Häcker, H., & Karin, M. (2006). Regulation and function of IKK and IKK-related kinases. *Science's STKE : Signal Transduction Knowledge Environment*, *2006*(357). https://doi.org/10.1126/STKE.3572006RE13/ASSET/A62405AE-2FA6-4C5C-9AF0-82332CB5D4F0/ASSETS/GRAPHIC/3572006RE13F6.JPEG

He, F., Antonucci, L., & Karin, M. (2020). NRF2 as a regulator of cell metabolism and inflammation in cancer. *Carcinogenesis*, *41*(4), 405–416. https://doi.org/10.1093/CARCIN/BGAA039

Ho, G. T., Porter, R. J., & Kalla, R. (2020). Ulcerative colitis: Recent advances in the understanding of disease pathogenesis. In *F1000Research* (Vol. 9). F1000 Research Ltd. https://doi.org/10.12688/f1000research.20805.1

Huber, A. K., Giles, D. A., Segal, B. M., & Irani, D. N. (2018). An emerging role for eotaxins in neurodegenerative disease. *Clinical Immunology (Orlando, Fla.)*, *189*, 29–33. https://doi.org/10.1016/J.CLIM.2016.09.010

Kang, S. H., Song, Y. J., Jeon, Y. D., Kim, D. K., Park, J. H., Soh, J. R., Lee, J. H., Kitalong, C., Kim, W., An, H. J., Chang, J. K., Lee, J., & Jin, J. S. (2021). Comparative Study of Anti-Inflammatory Effect on DSS-Induced Ulcerative Colitis Between Novel Glycyrrhiza Variety and Official Compendia. *Applied Sciences 2021, Vol. 11, Page 1545*, *11*(4), 1545. https://doi.org/10.3390/APP11041545

Kanmaniraja, D., Moreno, C. C., Moreno, R. D., & Shah, S. N. (2015). Approach to Colon Pathologies. In K. M. Elsayes (Ed.), *Cross-Sectional Imaging of the Abdomen and Pelvis: A Practical Algorithmic Approach* (pp. 369–401). Springer New York. https://doi.org/10.1007/978-1-4939-1884-3_12

Kelly, D., Conway, S., & Aminov, R. (2005). Commensal gut bacteria: Mechanisms of immune modulation. In *Trends in Immunology* (Vol. 26, Issue 6, pp. 326–333). https://doi.org/10.1016/j.it.2005.04.008

Kobayashi, T., Siegmund, B., Le Berre, C., Wei, S. C., Ferrante, M., Shen, B., Bernstein, C. N., Danese, S., Peyrin-Biroulet, L., & Hibi, T. (2020). Ulcerative colitis. *Nature Reviews Disease Primers*, *6*(1). https://doi.org/10.1038/s41572-020-0205-x

Krzystek-Korpacka, M., Kempiński, R., Bromke, M. A., & Neubauer, K. (2020). Oxidative Stress Markers in Inflammatory Bowel Diseases: Systematic Review. In *Diagnostics* (Vol. 10, Issue 8). Multidisciplinary Digital Publishing Institute (MDPI). https://doi.org/10.3390/diagnostics10080601

Laroui, H., Ingersoll, S. A., Liu, H. C., Baker, M. T., Ayyadurai, S., Charania, M. A., Laroui, F., Yan, Y., Sitaraman, S. V., & Merlin, D. (2012). Dextran Sodium Sulfate (DSS) Induces Colitis in Mice by Forming Nano-Lipocomplexes with Medium-Chain-Length Fatty Acids in the Colon. *PLOS ONE*, *7*(3), e32084. https://doi.org/10.1371/JOURNAL.PONE.0032084

Le Berre, C., Honap, S., & Peyrin-Biroulet, L. (2023). Ulcerative colitis. In *www.thelancet.com* (Vol. 402). www.thelancet.com

Li, Y. R., Jia, Z., & Trush, M. A. (2016). Defining ROS in Biology and Medicine. *Reactive Oxygen Species*, *1*(1), 9–21. https://rosj.org/index.php/ros/article/view/11

Llona-Minguez, S., Baiget, J., & Mackay, S. P. (2013). Small-molecule Inhibitors of IκB Kinase (IKK) and IKK-related Kinases. *Pharmaceutical Patent Analyst*, *2*(4), 481–498. https://doi.org/10.4155/PPA.13.31

Ma, H., Tao, W., & Zhu, S. (2019). T lymphocytes in the intestinal mucosa: defense and tolerance. In *Cellular and Molecular Immunology* (Vol. 16, Issue 3, pp. 216–224). Chinese Soc Immunology. https://doi.org/10.1038/s41423-019-0208-2

Mahadevan, V. (2020). Anatomy of the caecum, appendix and colon. *Surgery (Oxford)*, *38*(1), 1–6. https://doi.org/10.1016/J.MPSUR.2019.10.017

Mahon, M., Xu, J., Yi, X., Liu, X., Gao, N., & Zhang, L. (2016). Paneth Cell in Adenomas of the Distal Colorectum Is Inversely Associated with Synchronous Advanced Adenoma and Carcinoma. *Scientific Reports 2016 6:1*, *6*(1), 1–7. https://doi.org/10.1038/srep26129

Marrocco, I., Altieri, F., & Peluso, I. (2017). Measurement and Clinical Significance of Biomarkers of Oxidative Stress in Humans. *Oxidative Medicine and Cellular Longevity*, *2017*(1), 6501046. https://doi.org/10.1155/2017/6501046

Nandi, A., Yan, L. J., Jana, C. K., & Das, N. (2019). Role of Catalase in Oxidative Stress- and Age-Associated Degenerative Diseases. *Oxidative Medicine and Cellular Longevity*, *2019*, 9613090. https://doi.org/10.1155/2019/9613090

Pop, O. L., Vodnar, D. C., Diaconeasa, Z., Istrati, M., Bințințan, A., Bințințan, V. V., Suharoschi, R., & Gabbianelli, R. (2020). An overview of gut microbiota and colon diseases with a focus on adenomatous colon polyps. In *International Journal of Molecular Sciences* (Vol. 21, Issue 19, pp. 1–21). MDPI AG. https://doi.org/10.3390/ijms21197359

Qu, F., Xu, B., Kang, H., Wang, H., Ji, J., Pang, L., Wu, Y., & Zhou, Z. (2025). The role of macrophage polarization in ulcerative colitis and its treatment. *Microbial Pathogenesis*, *199*, 107227. https://doi.org/10.1016/J.MICPATH.2024.107227

Saez, A., Herrero-Fernandez, B., Gomez-Bris, R., Sánchez-Martinez, H., & Gonzalez-Granado, J. M. (2023). Pathophysiology of Inflammatory Bowel Disease: Innate Immune System. In *International Journal of Molecular Sciences* (Vol. 24, Issue 2). MDPI. https://doi.org/10.3390/ijms24021526

Salimoglu, S., Kilinc, G., & Calik, B. (2020). Anatomy of the colon, rectum, and anus. In *Colon Polyps and Colorectal Cancer: Second Edition* (pp. 1–22). Springer International Publishing. https://doi.org/10.1007/978-3-030-57273-0_1

Sellers, R. S., & Morton, D. (2014). The colon: From banal to brilliant. *Toxicologic Pathology*, *42*(1), 67–81. https://doi.org/10.1177/0192623313505930

Singh, V. P., Proctor, S. D., & Willing, B. P. (2016). Koch's postulates, microbial dysbiosis and inflammatory bowel disease. *Clinical Microbiology and Infection*, *22*(7), 594–599. https://doi.org/https://doi.org/10.1016/j.cmi.2016.04.018

Squire, J. D., & Leiding, J. W. (2022). Chapter 27 - Testing the adaptive immune system. In C. Chang (Ed.), *Allergic and Immunologic Diseases* (pp. 737–745). Academic Press. https://doi.org/https://doi.org/10.1016/B978-0-323-95061-9.00027-8

Stefano Corazziari, E. (2009). Intestinal mucus barrier in normal and inflamed colon. *Journal of Pediatric Gastroenterology and Nutrition*, *48*(SUPPL. 2). https://doi.org/10.1097/MPG.0b013e3181a117ea

Sun, L., Su, Y., Jiao, A., Wang, X., & Zhang, B. (2023). T cells in health and disease. In *Signal Transduction and Targeted Therapy* (Vol. 8, Issue 1). Springer Nature. https://doi.org/10.1038/s41392-023-01471-y

Ungaro, R., Mehandru, S., Allen, P. B., Peyrin-Biroulet, L., & Colombel, J. F. (2017). Ulcerative colitis. In *The Lancet* (Vol. 389, Issue 10080, pp. 1756–1770). Lancet Publishing Group. https://doi.org/10.1016/S0140-6736(16)32126-2

Wang, Z., Li, S., Cao, Y., Tian, X., Zeng, R., Liao, D. F., & Cao, D. (2016). Oxidative stress and carbonyl lesions in ulcerative colitis and associated colorectal cancer. In *Oxidative Medicine and Cellular Longevity* (Vol. 2016). Hindawi Publishing Corporation. https://doi.org/10.1155/2016/9875298

Wedel, T. (2017). Anatomy of the Colon, Rectum, Anus, and Pelvic Floor. In A. Herold, P.-A. Lehur, K. E. Matzel, & P. R. O'Connell (Eds.), *Coloproctology* (pp. 7–22). Springer Berlin Heidelberg. https://doi.org/10.1007/978-3-662-53210-2_2

Wen, C., Chen, D., Zhong, R., & Peng, X. (2023). Animal models of inflammatory bowel disease: category and evaluation indexes. *Gastroenterology Report*, *12*. https://doi.org/10.1093/GASTRO/GOAE021

Wirtz, S., Popp, V., Kindermann, M., Gerlach, K., Weigmann, B., Fichtner-Feigl, S., & Neurath, M. F. (2017). Chemically induced mouse models of acute and chronic intestinal inflammation. *Nature Protocols*, *12*(7), 1295–1309. https://doi.org/10.1038/nprot.2017.044

Yang, C., & Merlin, D. (2024). Unveiling Colitis: A Journey through the Dextran Sodium Sulfate-induced Model. In *Inflammatory Bowel Diseases* (Vol. 30, Issue 5, pp. 844–853). Oxford University Press. https://doi.org/10.1093/ibd/izad312

Yin, M., Wang, X., & Lu, J. (2020). Advances in IKBKE as a potential target for cancer therapy. In *Cancer Medicine* (Vol. 9, Issue 1, pp. 247–258). Blackwell Publishing Ltd. https://doi.org/10.1002/cam4.2678

Younus, H. (2018). Therapeutic potentials of superoxide dismutase. *International Journal of Health Sciences*, *12*(3), 88–93. https://pubmed.ncbi.nlm.nih.gov/29896077/

Yu, L. C. H. (2018). Microbiota dysbiosis and barrier dysfunction in inflammatory bowel disease and colorectal cancers: exploring a common ground hypothesis. In *Journal of Biomedical Science* (Vol. 25, Issue 1). BioMed Central Ltd. https://doi.org/10.1186/s12929-018-0483-8

Yu, Y., Liu, S., Yang, L., Song, P., Liu, Z., Liu, X., Yan, X., & Dong, Q. (2024). Roles of reactive oxygen species in inflammation and cancer. In *MedComm* (Vol. 5, Issue 4). John Wiley and Sons Inc. https://doi.org/10.1002/mco2.519

Yue, N., Hu, P., Tian, C., Kong, C., Zhao, H., Zhang, Y., Yao, J., Wei, Y., Li, D., & Wang, L. (2024). Dissecting Innate and Adaptive Immunity in Inflammatory Bowel Disease: Immune Compartmentalization, Microbiota Crosstalk, and Emerging Therapies. In *Journal of Inflammation Research* (Vol. 17, pp. 9987–10014). Dove Medical Press Ltd. https://doi.org/10.2147/JIR.S492079

Yunna, C., Mengru, H., Lei, W., & Weidong, C. (2020). Macrophage M1/M2 polarization. *European Journal of Pharmacology*, *877*, 173090. https://doi.org/10.1016/J.EJPHAR.2020.173090